# Technical University of Crete

## School of Electrical and Computer Engineering


Thesis

# Development of Spectral Data Estimation Methods Towards Expanding the Data Dimensionality in Spectral Imaging


*Author:*

Vassalos Konstantinos

*Committee:*

Dr. Costas Balas

Dr. Thrasyvoulos Spyropoulos

Dr. George Arvanitakis

# Abstract

HyperSpectral imaging is a technology that provides detailed spatial and spectral information about an object, combining spectroscopy with imaging capability. It captures detailed spectral information across the electromagnetic spectrum, obtaining the spectrum for each pixel in an image and enabling precise material identification and analysis. However, the high dimensionality of HyperSpectral data often poses significant challenges in terms of data acquisition, storage, and processing, particularly when aiming to achieve high spatial and spectral resolution simultaneously. This thesis focuses on the development of advanced HyperSpectral data estimation methods to enhance spectral resolution, reconstruct missing information, and expand the effective dimensionality of HyperSpectral datasets. To achieve this, we propose and evaluate computational techniques that leverage machine learning, signal processing, and mathematical modeling to improve HyperSpectral data estimation. These methods aim to reconstruct incomplete spectral signatures, enhance spatial and spectral resolution, and mitigate data acquisition limitations. The proposed approaches are tested on both synthetic and real HyperSpectral datasets, assessing their effectiveness in terms of accuracy, robustness, and computational efficiency.

# Acknowledgments

After 5 years of hard but at the same time exciting work and before I present my thesis, I want to express my deepest gratitude to all the people that helped me in this academic journey and made everything I achieved possible.

First and foremost, i have to thank my advisor Professor Costas Balas for his unwavering support and invaluable guidance throughout the development of this thesis. His insightful feedback, constructive critiques, and patient encouragement have significantly shaped both the direction and the quality of my work. I am also grateful towards the other two members of the committee Professor Thrasyvoulos Spyropoulos and Dr. George Arvanitakis for being part of this thesis.

I couldn't achieve anything without the support of my family. I would like to thank my parents, Nektarios and Evangelia, for their unconditional support and for sacrificing so much in order to help me be in this position today. Also my sister, Stella, that paved the 'academic way' for me to walk on and showed me that nothing is unreachable.

Also, I would like to thank my girlfriend, Despoina, for her steady support throughout long hours of study for this thesis. Her confidence in my abilities, patience and encouragement have meant more to me than words can fully describe.

Lastly I wish to thank all my close friends for their advising and support throughout all these years of my studies. All of you made this journey unforgettable.

# Contents

# List of Figures

# List of Tables

# Chapter 1

# Introduction

## 1.1 Introduction to Spectral Data Estimation

In recent years, the development in the field of optical imaging has been rapid, and the color imaging systems that have been developed have reached a very high resolution, enabling 3D images. These systems work by producing three dimensional data(most of the times this data represent RGB) where each dimension represents the intensity and chrominance of light.

Even though color imaging systems offer very good resolution of the scenes they capture, they miss a significant amount of information that they are unable to detect. This information is hidden in the bands within the UV or infrared regions of the spectrum, and in many cases, it is the most critical. That's why spectral imaging systems are used, so this hidden information is obtained.

Spectral imaging is a transformative technology that captures spatially resolved spectral information across a wide range of wavelengths, enabling detailed material characterization, environmental monitoring, medical diagnostics, and industrial quality control. By combining spatial and spectral di-

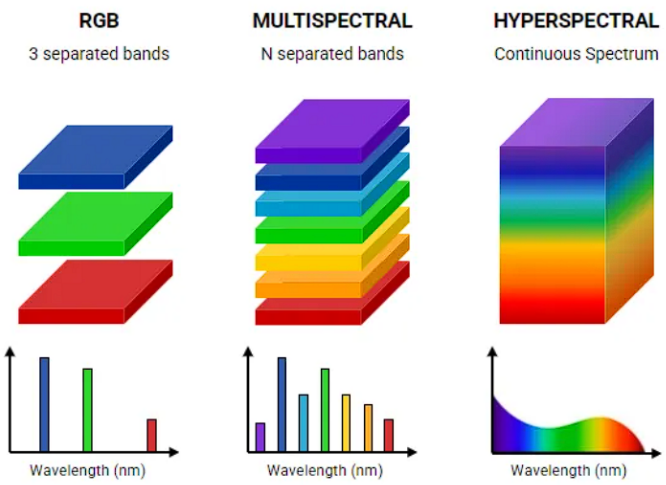


Figure 1.1: RGB (left) and MultiSpectral (center) imaging only provide discrete and discontinuous portions of the spectral range. HyperSpectral imaging (right) creates a hypercube, which yields the complete and continuous spectrum for each pixel of the image.[1]

mensions, spectral imaging systems generate datasets that reveal the unique "fingerprint" of materials based on their light-matter interactions. Essentially, spectral imaging combines two disciplines - spectroscopy and photography - to sample image data at many wavelength bands. In general SI is separated in 2 categories: MultiSpectral imaging(<20 wavelength bands sampled) and HyperSpectral imaging (>20 wavelength bands sampled). The choice of which is best for use depends on the level of accuracy that is required or the time that is available.

However, the acquisition of high-dimensional spectral data (e.g., HyperSpectral or MultiSpectral cubes) is often constrained by practical limitations, including sensor resolution, data storage, and acquisition time. These challenges have spurred the development of spectral imaging data estimation, a computational framework aimed at reconstructing, enhancing, or extrapolating spectral information to overcome hardware limitations and expand data dimensionality.

## 1.2 Spectroscopy/Spectrometry

Spectroscopy studies the absorption and emission of light and other radiation by matter, as related to the dependence of these processes on the wavelength of the radiation, enabling the identification and characterization of materials based on their unique spectral signatures. The definition was expanded to include the study of interactions between particles such as electrons, protons, and ions, as well as their interactions with other particles as a function of wavelength ($\lambda$) or frequency (v). In the context of spectral imaging, spectroscopy principles are extended spatially, allowing pixel-level spectral analysis to map material distributions in complex scenes.

Spectrometry is the measurement of the interactions between light and matter, and the reactions and measurements of radiation intensity and wavelength. In other words, spectrometry is a method of studying and measuring a specific spectrum, and it's widely used for the spectroscopic analysis of sample materials. The instrument used to perform such measurements is called a spectrometer or spectrograph.

Both of them are used in chemistry for the identification of substances through the spectrum emitted from or absorbed by them. Also they find usage in astronomy and remote sensing.

## 1.3 Wave-particle duality, Photoelectric Effect

By now, it is common knowledge that light, one of the most important phenomena of electromagnetism, has a dual nature. It can behave as a wave or as a photon particle, depending on the circumstances and the effect being observed. This duality was first conceptualized by Einstein in his explanation

of the photoelectric effect, a phenomenon that classical wave theory could not fully explain. When it behaves like a wave, light is emitted and propagated and when it behaves like a particle, light is absorbed. The photoelectric effect occurs when light (or electromagnetic radiation) strikes a material causes the ejection of electrons from its surface. Light, as an electromagnetic wave, has both electric and magnetic field components, which oscillate in a fixed relationship to one another, perpendicular to each other and perpendicular to the direction of the energy and wave propagation.

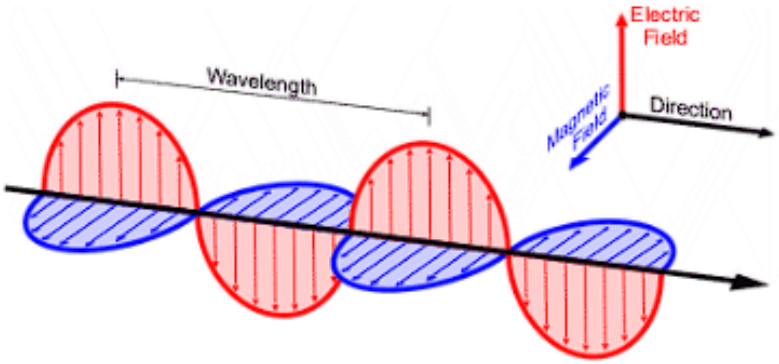


Figure 1.2: Electromagnetic Wave [2]

## 1.4 Electromagnetic Spectrum

Electromagnetic waves are categorized according to their frequency $f$ or, equivalently, according to their wavelength $\lambda = \frac{c}{f}$.Visible light makes up just a small part of the full electromagnetic spectrum. Electromagnetic waves with shorter wavelengths and higher frequencies include ultraviolet light, X-rays, and gamma rays. Electromagnetic waves with longer wavelengths and lower frequencies include infrared light, microwaves, and radio and television waves.

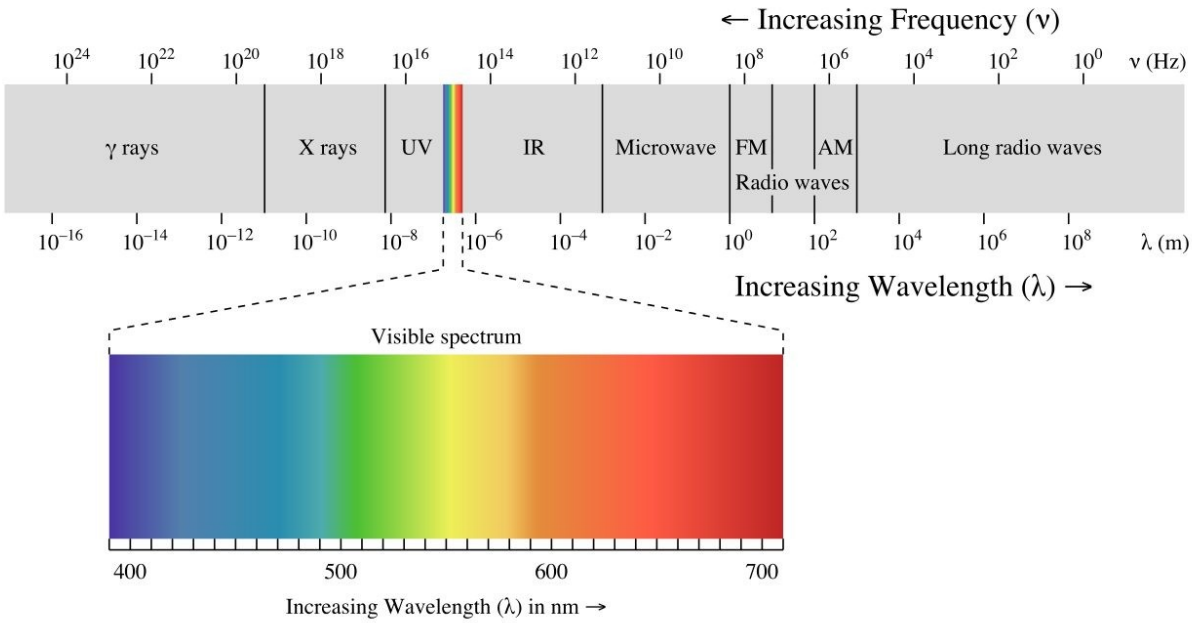


Figure 1.3: Electromagnetic Spectrum [3]

## 1.5 Spectral Imaging

Spectral imaging is the application of reflectance spectroscopy to every pixel in a spatial image, integrating spatial and spectral information to characterize materials and scenes across a wide range of wavelengths. It finds a lot of applications in different fields like art conservation, astronomy, solar physics etc. For example, imaging spectrometers are used in planetary observations to study the Earth from orbiting satellites. The spectrometer functions by recording all points of color on a picture, thus, the spectrometer is focused on specific parts of the Earth's surface to record data. The advantages of spectral content data include vegetation identification, physical condition analysis, mineral identification for the purpose of potential mining, and the assessment of polluted waters in oceans, coastal zones and inland waterways.

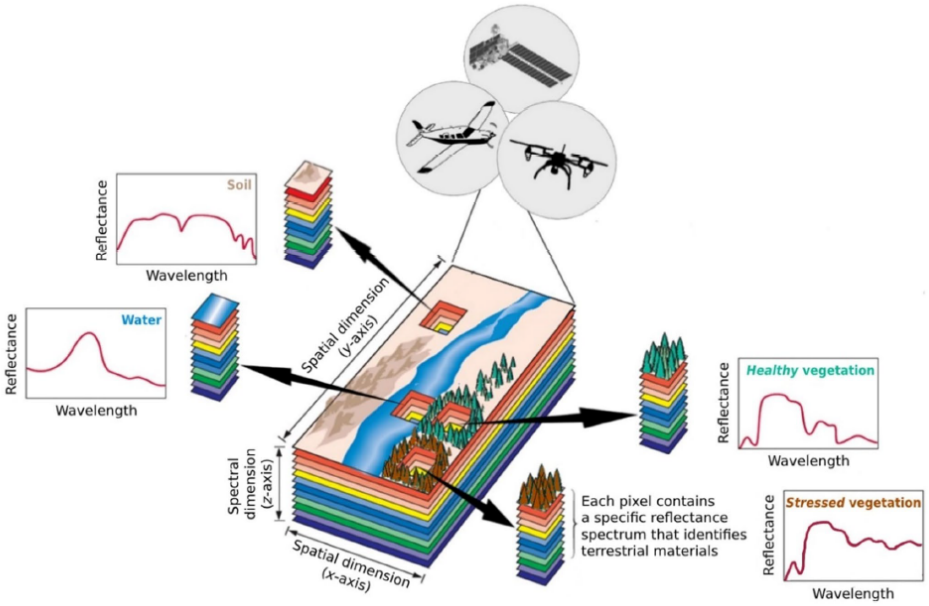


Figure 1.4: Principle of imaging spectroscopy. Space and airborne imaging spectral sensors provide spectral information with spatial resolution of the imaged object [4]

## 1.6 HyperSpectral Imaging

HyperSpectral imaging collects and processes information across the electromagnetic spectrum. HyperSpectral imaging, in contrast to the human eye, which sees only visible light, can detect and process light from the ultraviolet to the infrared. This allows for the identification of objects and materials by analyzing their unique spectral signatures. Applications of HyperSpectral imaging include food quality and safety, waste sorting and recycling, and control and monitoring in pharmaceutical production.

By combining the benefits of digital imaging and a spectrometer, HyperSpectral imaging provides both spatial and spectral information about the object's physical and chemical properties. The spectral information allows for the identification and classification of materials and the spatial provides data on the material's distribution and areal separation. HyperSpectral imaging

provides answers to questions concerning "what" (based on the spectrum), "where" (based on location), and "when".

A HyperSpectral camera measures thousands or hundreds of thousands of spectra to create a massive HyperSpectral data cube comprising position, wavelength, and time-related information. Every object leaves a unique "fingerprint" across the electromagnetic spectrum. These "fingerprints" are known as spectral signatures and are used for the identification of the materials.

Compared to MultiSpectral imaging, HyperSpectral imaging provides more information allowing more accurate analysis, identification, and separation of materials and substances.

## 1.7 HyperSpectral Data acquisition

The main problem when recording spectral images is that often the systems require a longer duration to record the spectral cube than the duration of the phenomena being observed. This means that due to scene movement, some critical information cannot be recorded. This happens because these systems record spectral images one after the other and then assemble the images to obtain the spectra.

First, the simplest one is the point scanning method(whiskbroom scanning), where a single point is scanned along two spatial dimensions by moving either the detector or the sample. All the data are accumulated in an exhaustive sequence, pixel by pixel. Even though this technique is accurate, it is characterized by really low speed.

The second technique is line scanning(Pushbroom scanning) and is an extension of point-scanning. In this method, a slit of spatial information as well as spectral information for each spatial point is acquired. Ξven though it is faster than the point scanning it requires perfect alignment and is sensitive to object's motion.

Another method is the area scanning(band sequential scanning) which is a spectral scanning method. This method acquires a single band image with full spatial information at once. Then a spectral Cube containing a stack of single band images is created using different wavelength images. This method also is pretty slow considering that it has to take images from hundreds of different wavelengths.

Finally, the last technique is the single shot scanning(SNSI) with only one exposure. This method records both spectral and spatial information on an area detector at the same time which means it has fast acquisition of accurately registered images making it very appealing. The main problem is that, because of the technological limitation there is a trade-off between spatial and spectral resolution.

Summing up, the first three scanning methods are more suitable when stationary and invariant scenes are the ones that are captured due to the fact that they have better satial and spectral resolution. The single shot scanning, is the only solution if the scene that is captured is dynamically developed.

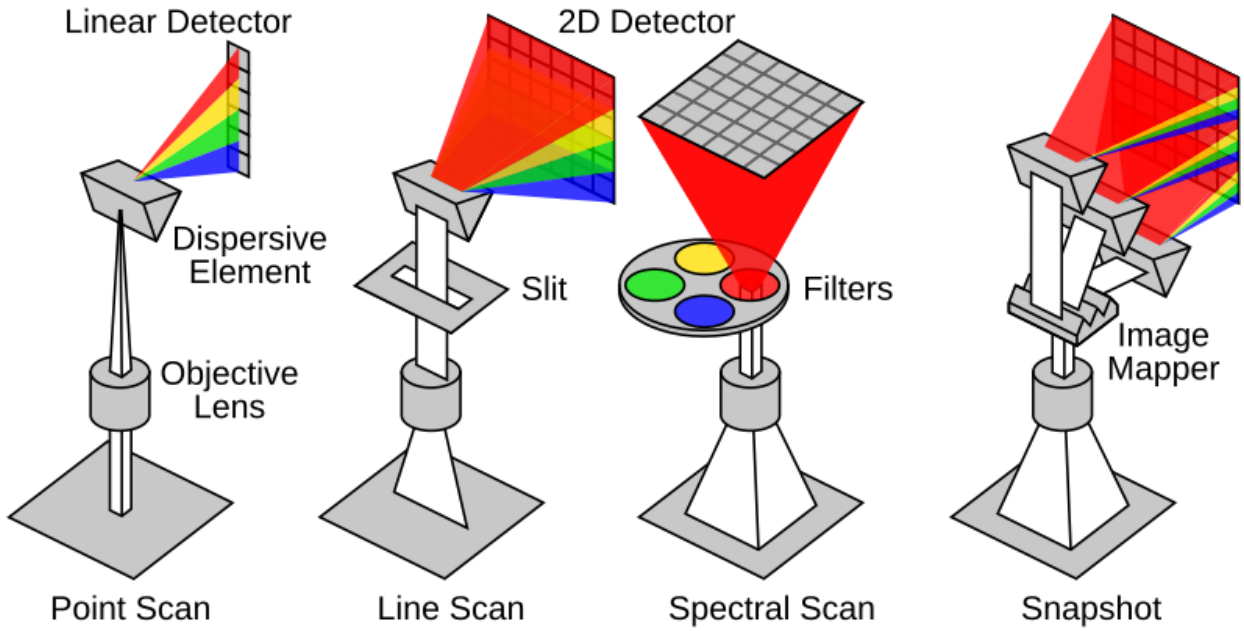


Figure 1.5: Spectral imaging approaches.[5]

## 1.8 Spectral Cubes

Most of the time, information collected from spectral imagers is processed based on the application and then stored in a 3D data structure called a spectral cube for further analysis. This cube consists of a large number of consecutive and registered sets of spectral images. The first two dimensions respond to spatial dimensions which is the pixel coordinates and the third dimension refers to the spectral dimension which contains a specific wavelength of the electromagnetic spectrum. A spectral cube is created through a process that combines spatial imaging with spectral data acquisition.

These Cubes are created by a series of consecutive sub-images one stacked behind the other each taken at different wavelength. Each image provides the spatial distribution of the spectral intensity at a certain wavelength.

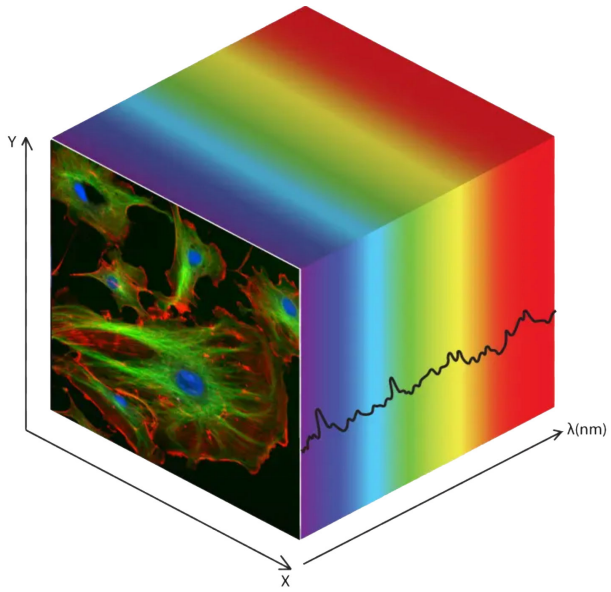


Figure 1.6: The front face of this 3D spectral cube maps three wavelengths to red, green, and blue. The third dimension shows surface-reflected solar radiation wavelength [6]

## 1.9 Color Imaging vs spectral imaging

Color imaging systems use sensors, typically based on CCD(Charge-Couple Device) or CMOS(Complementary Metal-Oxide-Semiconductor) technology, to detect light. These sensors have a Bayer filter, that let only green, red and blue spectral bands throw emulating the human vision. Just like the human eye, these sensors have limitations associated with the loss of information. They allocate all incoming light into only three RGB coordinates, entirely missing the important information hidden in other spectra. That means that objects with the same RGB values are categorized as the same despite even if they have different spectral components. This phenomenon is known as metamerism. Due to this effect, these color imaging systems don't have the ability to distinguish material with the same color appearance but different chemical composition. In contrast, spectral imaging systems captures different images in different wavelengths of a pixel, so the unique fingerprint of

each object could be extracted and the metamerism effect almost disappears.

## 1.10 MultiSpectral vs HyperSpectral imaging

The main difference between MultiSpectral and HyperSpectral imaging is the number of the bands that are used and also how narrow the bands. MultiSpectral imaging takes multiple images at discrete and narrow bands. MultiSpectral imaging systems differ from color imaging systems in the way that they capture more spectra than simple RGB but do not produce the full spectrum of the object. On the other hand, HyperSpectral sensors measure the energy in a vastly bigger number of bands and also narrower bands and at the end they produce the spectra all the pixels that are in the scene. All of the bands together produce a continuous spectrum across almost the entire electromagnetic spectrum and for that reason they are more sensitive to variations in reflected energy.

## 1.11 HyperSpectral imaging Application

As technology develops, HyperSpectral imaging provides more and more applications in a big variety of subjects and studies. This is, because the spectral information that is being revealed from HyperSpectral imaging gives a lot more information that the human eye or systems that work with color imaging(RGB) could ever provide. A few of these applications are provided below.

HSI plays a very important role in environmental monitoring. Its ability to capture and translate spectral details allows researchers and scientists to get a very good understanding of the parameters they are monitoring, which

in different case couldn't observe. They enable large-scale mapping of areas using satellites or airborne systems, which would otherwise be difficult or impossible to access, allowing remote monitoring. Also, satellite imagery provides information with a very high accuracy enabling the identification of subtle changes and features, that might be missed by other imaging methods.

Another important application of HSI is on pharmaceutical products and medical science. Pharmaceutical products are very often too similar for the human eye to identify any difference, despite having very different chemical compositions. HSI provides a reliable, rapid and non invasive way to analyze the chemical composition of drug formations such as tablets and capsules. So, it enables the identification of the products that looks exactly the same, but have different dosages by analyzing the active ingredient distribution. In medical science, HSI systems shows a very high potential as a diagnostic tool in many medical applications. Non-contact skin measurements with a HyperSpectral camera can give reliable information about tissue health through e.g., oxygenation and blood circulation efficiency, help in an open wound and burn wound diagnostics, and identify cancer tumors or blood circulation problems related to diabetes.

HSI systems, also, find use in food quality and safety industry. They can detect defects and abnormalities in food products that are not visible to the human eye. They are able to analyze large volumes of products in real time and obtain the chemical information across the entire product stream by detecting the different quality parameters simultaneously with a single scan.

Mineral exploration is another field that HSI is being used vastly. HSI provides powerful and advanced solutions for the mining and oil industries

enabling more efficient mineral exploration and higher automated mining production processes with reduced waste streams and energy consumption. It has been used for mineral exploration from the air over large groups of rocks that makes visibility impossible for a long time. Now, it is applied as a method for reliable mineral analysis in drill cores and other geological samples. In the infrared region HSI reveals alteration patterns that can't be seen in traditional logging by the human eye. Almost all minerals can be objectively and consistently identified and mapped in the infrared region.

## 1.12 Spectral Estimation

By now, it is established that the main limitation of RGB imaging devices is their inability to capture important information hidden in other spectra. Another significant disadvantage of RGB imagers, is that objects with different spectral information may have the same RGB values, resulting in the inability of RGB devices to detect chemical differences.

Spectral Estimation is a computational process used to reconstruct, enhance, or predict spectral information from incomplete or noisy data. In the context of spectral imaging, it involves estimating the full spectral signature of a scene or object, when only partial or low-resolution spectral data is available. This is particularly important in applications where hardware limitations, such as sensor resolution or data acquisition time, restrict the ability to capture high-quality spectral data directly.

Spectral Estimation is also beneficial in memory saving due to the fact that a very small amount of bands need to be saved in order for the full spectrum to be recovered.

Spectral Estimation techniques leverage mathematical models, signal processing algorithms, and machine learning to infer missing spectral details. For example, in HyperSpectral imaging, spectral estimation can be used to reconstruct high-resolution spectral cubes from undersampled data or to enhance the spatial and spectral resolution of captured images.

The main reason why the estimation is happening in the spectral domain, and not in the spatial domain lays on the nature of these domains. Spatial domain is characterized by features with high intensity (i.e corners), that are those that change greatly in intensity over short image distances. Because of the non periodic nature of those differences it is extremely hard for an estimation algorithm to estimate the missing information and reconstruct the actual scene. Spectral domain on the other hand is much more predictable because most of the signals that are in the 400nm-1000nm wavelength only have a few peaks and valleys.

Most of the HSI devices, that are build now, already have the mentioned trade off between spectral and spatial resolution, that is created due to hardware limitations. As the spectral bands increases the spatial resolutions decreases and vice versa, so the missing information is a strategic decision, that the designers of HSI devices have to make, that depends on the goals and the accuracy they are trying to achieve. Choosing to save the spatial resolution we will try to find ways to expand the data dimensionality in spectral imaging systems by finding appropriate estimation algorithms in terms of minimizing the estimation error.

# Chapter 2

# Spectral Estimation

## 2.1 Introduction

As we described in the previous chapter, HyperSpectral imaging is a very promising technology that includes both conventional imaging and spectroscopy, in order to extract information about the spatial, as well as the spectral domain of an object or a scene. The importance of the information that HSI provides in so many different fields, such as bio-medical technology, remote sensing etch. must be well established by now. However, the research that has been made around HSI this far hasn't found a solution for some crucial things in HSI systems. The acquisition time, as well as the cost and the size of those systems are still some factors that don't allow HSI systems to observe any dynamically developing phenomena. In order to overcome these problems, researchers are trying to estimate the spectral domain of the spectral cube by using digital RGB sensors. By using some typical RGB cameras and taking millions of measurements in order to estimate some of the spectral properties, like color, they manage to produce a close enough estimation, while keeping a lower cost, by a significant amount, from the traditional HSI systems. Obviously, the accuracy of these sensors is not close to the accuracy that a HSI system would produce, but the large difference in

the equipment cost is worth it for some relatively simple use. Due to the fact that the difference in cost is really big, a lot of research has been made in ways that could improve the precision of the spectral estimation, while using RGB sensors. Most of the studies use fixed RGB hardware and then try to make improvements by creating better postprocessing algorithms. The goal is to produce the best spectral reconstruction of the object by expanding the data dimensionality using machine learning algorithms.

A lot of different methods have been proposed in order to estimate the spectral reflectance of a three-band image. The most used method for spectral reflectance estimation is Wiener and pseudoinverse method [10]. This method finds a lot of use in different fields [11] [12] [13]. Another alternative of Wiener estimation method was proposed by Murakami[14]. A three-band image is divided into several blocks and the spectral estimation is carried out using the Wiener estimation matrix assigned to each block. In [15] a new spectral reconstruction method was proposed, called the matrix R method. This method combines the benefits of both colorimetric and spectral transformations. Tristimulus values were predicted by a colorimetric transformation from multi-channel camera signals, while spectral reflectance factor was estimated by a spectral transformation from the same signals. The method reconstructed reflectance factor, by combining the fundamental stimulus from the predicted tristimulus values with the metameric black from the estimated spectral reflectance, based on the Wyszecki hypothesis [16]. Other methods for reconstructing spectral images from RGB has been explored, with sparse reconstruction methods and different types of neural networks. Sparse reconstruction methods uses the idea that most of the information in a spectral signal can be represented using only a small number of significant coefficients in a suitable basis or dictionary[17] [18]. Another promising method, that has

been introduced, is the A++ algorithm that uses pixel-based processing [19] . Deep convolutional neural networks(CNN) [20][21] and self-supervised assisted semi-supervised residual network (SSRNet) [22] are some of the DNNs that have been used to reconstruct spectral images. As we will see in following sections, DNN performance is only slightly better than the much simpler pixel-based methods, where spatial context is not used.

As we mentioned before, the main problem with RGB sensors is that they are only able to obtain 3 spectral images, so it is a hard task to generate all of the other missing spectra. With that said, it's easy to understand that all the methods, that have been, mentioned have some limitations when it comes to the result they can produce, due to the low number of features. Other techniques like using MultiSpectral cameras and multiple spectral sources[23] or using a library-based Dictionary learning algorithm [24] have been proposed. Also, methods using different kind of lenses, like diffractive lenses, have also been studied [25] . An interesting study [26] was conducted using 16 narrow band wheel-filter MultiSpectral camera that can uniformly cover the visible spectrum and the partial least squares methods for estimating the missing spectral images, producing a better result that Wiener estimation and polynomial regression. The main downside of all the above techniques, that are non-snapshot related, is the fact that they cannot observe dynamically developed phenomena, due to the long time that is needed for them to get all the images. Some articles, that try to reach real time spectral reconstruction, are working with various techniques like fast-N-Squeeze [27] in which, given an input image, our method determines a global RGB-to-spectral linear transformation matrix, based on a search through optimal matrices from training images, that share low-level features with the input. The resulting spectral signatures are then adjusted by a global scaling factor, determined through

a lightweight SqueezeNet-inspired neural network.

The goal of this thesis is to compare different techniques, that are used for data dimensionality expansion using spectral data estimation and will give a very strong focus on the time that each algorithm needs to execute. The methods will be compared in terms of minimizing the root mean square reconstruction error(RMSE), because this is the standard comparison that is being used in most of the studies. Many methods are compared, linear and non-linear, using images taken in the lab with a MultiSpectral camera. Our ultimate goal is to estimate HyperSpectral images from MultiSpectral ones in a short amount of time and with as smaller error as possible.

## 2.2 Mathematical models for similarity comparison

In this section, different mathematical models are used, in order to measure the similarity of the original reflectance and the estimated reflectance will be introduced. Not all of the available metrics will be covered, but only the most well known and most commonly used for the benchmark of spectral reconstruction methods and more in general for the assessment of similarity between spectra.

### 2.2.1 Euclidean Distance

In mathematics, the Euclidean distance between two points in Euclidean space is the length of the line segment between them. This distance can be be also expressed in terms of the Euclidean norm of the Euclidean vector difference.

$$ED(R(x,\lambda),\hat{R}(x,\lambda)) = ||(R(x,\lambda) - \hat{R}(x,\lambda)|| = \sqrt{\Sigma_x||(R(x,\lambda) - \hat{R}(x,\lambda)||_2^2}$$

### 2.2.2 Mean squared error measures

A very important group of measures consists of what could be called mean error measurements, which are all based on an euclidean measure of the error between recovered and ground-truth spectra. Measures belonging to this group are: the Mean Square Error (MSE), the Root Mean Square Error (RMSE), the Mean Relative Absolute Error (MRAE), which operates in the spectral domain and its correspondent in the RGB domain, which is the Back-Projection MRAE (BPMRAE) [21], and the Peak Signalto-Noise Ratio (PSNR). The definitions of the previous measures are the following:

$$MSE = \frac{\sum_x \|R(x,\lambda) - \hat{R}(x,\lambda)\|_2^2}{N}, \tag{2.1}$$

$$RMSE = \sqrt{MSE}, \tag{2.2}$$

$$MRAE = \frac{1}{N}\sum_{x,\lambda} \frac{|R(x,\lambda) - \hat{R}(x,\lambda)|}{R(x,\lambda)}, \tag{2.3}$$

$$BPMRAE = \frac{1}{N}\sum_{x,\lambda} \frac{|\mathrm{CRF} \times R(x,\lambda) - \mathrm{CRF} \times \hat{R}(x,\lambda)|}{\mathrm{CRF} \times R(x,\lambda)}, \tag{2.4}$$

$$PSNR = 20 \times \log_{10}\left(\frac{p_{max}}{MSE}\right). \tag{2.5}$$

where $R(x,\lambda)$ and $\hat{R}(x,\lambda)$ are the actual and the reconstructed spectral reflectances, N is the size of the actual image(pixel count $\times$ number of spectral channels), CRF is the camera response function and $p_{max} = 2^{16}$ i.e 65,535, corresponds to the maximum possible value of each pixel.

### 2.2.3 Goodness-of-Fit Coefficient (GFC)

This measure instead of computing the euclidean distance, estimate the similarity between recovered spectra and ground truth.

$$GFC = \frac{1}{N}\Sigma_x \frac{|\Sigma_\lambda R(x,\lambda)\hat{R}(x,\lambda)|}{\sqrt{\Sigma_\lambda [R(x,\lambda)]^2}\sqrt{\Sigma_\lambda [\hat{(}x,\lambda)]^2}} \tag{2.6}$$

### 2.2.4 Angular measurements

This group of measures, measure the angle between the recovered and ground-truth spectra. This way, the focus is more on the shape of the spectra than on their absolute values. To this group belong 2 measures : Spectral Angle Mapper (SAM) [10], Mean Angular Error (MAngE). SAM calculates the average spectral angle between the spectra of the actual and the reconstructed HyperSpectral images. The spectra are treated as vectors in a space with dimensionality equal to the number of bands. It is based on this equation:

$$SAM = \frac{1}{m}\cos^{-1}\left(\sum_{j=1}^{m}\frac{\left(p_h^{(j)}\right)^T p_c^{(j)}}{\|p_h^{(j)}\|_2 \, \|p_c^{(j)}\|_2}\right). \tag{2.7}$$

$p_h^{(j)}$, $p_c^{(j)} \in \mathbb{R}^C$ represent the spectra of the $j$-th HyperSpectral pixel in real and estimated HyperSpectral images ($C$ is the number of bands), and $m$ is the total number of pixels within an image. MAngE is expressed by the formula:

$$MAngE = \frac{1}{N}\sum_i angle(r_i, \hat{r}_i). \tag{2.8}$$

All of the above metrics can be found in [28].

## 2.3 Spectral Model of Acquisition- Problem Statement

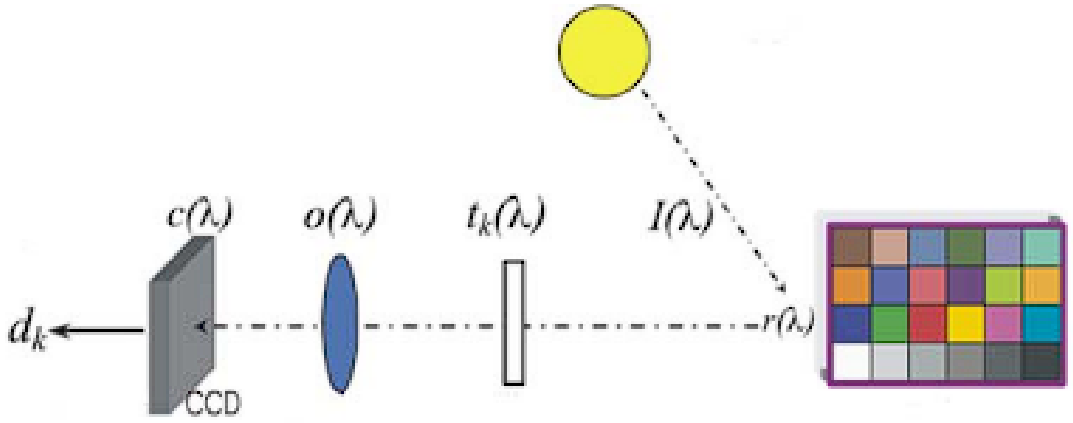


Figure 2.1: Synopsis of the spectral model of the acquisition process in color/MultiSpectral systems [7].

The acquisition process in a MultiSpectral imaging system involves multiple components that can be seen in the 2.1 , I(λ) is the spectral radiance of the illuminant, r(λ) is the spectral reflectance of the surface, o(λ) is the spectral transmittance of the optical system, $t_k(\lambda)$ is the spectral transmittance related to the $k^{th}$ filter and c(λ) is the spectral sensitivity of the camera. A spectral noise $n_k$ is added for the $k^{th}$ channel,$k = 1...K$. The camera output $d_k$ related to the channel k for a single pixel of the image is given by

$$d_k = \int_{\lambda_{max}}^{\lambda_{min}} I(\lambda)r(\lambda)o(\lambda)c(\lambda)t_k(\lambda)\,d\lambda + n_k \tag{2.9}$$

If we assume that there is no noise by preprocessing and assuming a linear opto-electronic transfer function, we can replace I(λ), c(λ), o(λ), $t_k(\lambda)$ by the spectral sensitivity $S_k(\lambda)$ of the $k^{th}$ channel. Then, 2.9 can be written as :

$$d_k = \int_{\lambda_{max}}^{\lambda_{min}} S_k(\lambda)r(\lambda)\,d\lambda \tag{2.10}$$

where $S_k = [S_k(\lambda_1), S_k(\lambda_2), ..., S_k(\lambda_p)]^T$ is a column vector containing the spectral sensitivity of the acquisition system related to the $k^{th}$ channel of a single pixel and $r = [r(\lambda_1), r(\lambda_2), ..., r(\lambda_p)]^T$ is a column vector of the sampled spectral reflectances of the scene. If we have a system that has all channels, we can rewrite 2.10 as

$$\mathbf{d} = \mathbf{S}^T\mathbf{r} \tag{2.11}$$

where $\mathbf{d}$ is the vector containing all $d_k$ camera outputs and $\mathbf{S}= [s_1, s_2, ..., s_K]^T$ is the matrix containing the channels spectral sensitivities $\mathbf{S}_k$. The final goal is to recover $\mathbf{r}(\lambda)$ from the camera output given by 2.11. This can be done by finding an operator $\mathbf{Q}$ that satisfies

$$\widetilde{r} = \mathbf{Q}\mathbf{d} \tag{2.12}$$

Depending on how the matrix S is determined, three main paradigms of spectral reflectance estimation exist.

- If $\mathbf{S}$ is obtained by a direct physical system characterization, the operator $\mathbf{Q}$ is the inverse or the pseudo-inverse of $\mathbf{S}$. Thus, $\mathbf{Q}=\mathbf{S}^+$, where + is the pseudo-inverse operator.

- If $\mathbf{S}$ is obtained indirectly by matching a set of $M$ color patches (for which we know the theoretical reflectance)and an image of these patches is captured by the camera, then we have a set of corresponding pairs ($d_m$,$r_m$), for m=1,...,M, where $\mathbf{d}_m$ is a vector of dimension K containing the camera responses, and $\mathbf{r}_m$ is a vector of dimension $N$ representing the spectral reflectance of the $\mathbf{m}^{th}$ patch. The reflectances $\mathbf{r}_m$ are gathered in the matrix $\mathbf{R}$ and the camera outputs for the $M$ patches are gathered in the matrix $\mathbf{D}$, so 2.11 can be rewritten as $\mathbf{D} = \mathbf{S^T R}$. The operator $\mathbf{Q}$

is directly obtained by calculation of this matching. Any optimization method can fulfill this aim (neural networks, least squares regression...). Thus, the operator $\mathbf{Q}$ is obtained from

$$\mathbf{R}=\mathbf{QD} \tag{2.13}$$

through the pseudo-inverse of $\mathbf{D}$

$$\mathbf{R}=\mathbf{QD}^{+} \tag{2.14}$$

which as $J$=$K$ becomes

$$\mathbf{Q}=\mathbf{RD}^{-1} \tag{2.15}$$

- The third paradigm for spectral reflectance estimation consists of directly interpolating the camera outputs $\mathrm{d}_k$. Thus, no knowledge about the matrix $\mathbf{S}$ is required. However, rigorous conditions about filters' shapes and numbers make this technique ineffective for reflectance estimation from color cameras.

The focus of this study, will be on the second paradigm (learning from examples). This paradigm is also referred to as overdetermined problem.

The optimal $\mathbf{Q}$ is determined by minimizing the mean square error (MSE) between the true reflectance $\mathbf{r}$ and its estimate $\tilde{\mathbf{r}}$.

$$\arg\min_{Q} E\{\|\mathbf{r}-\mathbf{Q}\mathbf{d}_m\|^2\}. \tag{2.16}$$

Assuming that the camera output $\mathbf{d}$ is related to the reflectance $\mathbf{r}$ via a linear model (and, if needed, including an additive noise term n) as

$$d = Sr + n \tag{2.17}$$

where S is the matrix containing the spectral sensitivities of the camera channels and n is a zero-mean noise vector, the solution for $\mathbf{Q}$ is obtained by setting the derivative of the error function with respect to $\mathbf{Q}$ equal to zero.

## 2.4 Spectral Estimation Algorithms

### 2.4.1 Wiener method

The Wiener estimation method is one of the most well-known algorithms in the field of spectral estimation [10]. The purpose of the Wiener estimation is to make estimations from low-dimensional data into high dimensional data, for example, from three-filter camera responses into reflectance spectra. The goal of the Wiener method is to estimate the matrix $\mathbf{Q}$ in order to minimize the square error between reference $\mathbf{r}_o$ reflection and the estimated $\mathbf{r}$.

Now, solving 2.16 with the Wiener method we get:

$$\mathbf{Q}^{\text{Wiener}} \approx R_{rr}S^T(SR_{rr}S^T + R_{nn})^{-1}$$

where $R_{rr}$ is the auto-covariance of the reflectance, $S$ is the camera sensitivity matrix, and $R_{nn}$ is the noise covariance.

Given training data, we estimate the covariances empirically:

$$R_{rr} \approx \frac{1}{M}RR^T, \qquad R_{nn} \approx nI$$

where $R$ is the matrix of training reflectance spectra and $M$ is the number of training samples.

The camera response data is $D = SR$, so:

$$SR_{rr}S^T \approx \frac{1}{M}DD^T$$

$$R_{rr}S^T \approx \frac{1}{M}RD^T$$

Substituting these into the Wiener formula gives:

$$\mathbf{Q}^{\text{Wiener}} \approx \frac{1}{M}RD^T\left(\frac{1}{M}DD^T + nI\right)^{-1}$$

Multiplying numerator and denominator by $M$ yields:

$$\mathbf{Q}^{\text{Wiener}} \approx RD^T(DD^T + MnI)^{-1}$$

Alternatively, depending on the data arrangement, the empirical solution may be written as:

$$\mathbf{Q}^{\text{Wiener}} \approx \frac{1}{M^2}(D^T D + n)^{-1} D^T R$$

where $D$ and $R$ are the data matrices of sensor responses and reflectances, respectively, and $n$ is a regularization parameter.

In this method, the **training phase** involves computing the statistical properties of the data, specifically the mean spectrum, the autocorrelation matrix of the reflectance ($R_{rr}$), and the noise covariance ($R_{nn}$). These are estimated from a set of reference spectra . The result of the training phase is the pre-computed Wiener gain matrix $\mathbf{Q}^{Wiener}$, which encapsulates the optimal linear mapping from sensor responses to reflectance spectra under the assumed noise and data statistics.

During the **estimation phase**, this pre-computed matrix $\mathbf{Q}^{Wiener}$ is used to transform new, unseen sensor measurements (e.g., from a camera) into estimated reflectance spectra. The estimation itself is a simple matrix multiplication, which is computationally efficient and does not require re-training or re-computation of the statistical matrices.

Therefore, the **training phase** learns the statistical relationships and computes the Wiener matrix, while the **estimation phase** applies this matrix to new measurements to obtain spectral estimates.

The time complexity of Wiener method is O(NK), where K is the number of camera responses and N is the spectral reflectances. The training phase requires a constant number of multiplications because it takes place only one time.

### 2.4.2 Multivariate Linear Regression Method

Linear Regression is a statistical method used to model the relationship between a dependent variable and one or more independent variables. It computes the linear relationship between the dependent variable and one or more independent features by fitting a linear equation with observed data. It predicts the continuous output variables based on the independent input variable. Multivariate linear regression involves more than one independent variable and one dependent variable. In this problem the aim is to establish a linear relationship between the spectral reflectance $\mathbf{r}$ and the camera responses $\mathbf{d}$. The model assumes that $\mathbf{r}$ can be expressed as a linear transformation of $\mathbf{d}$ with an estimation matrix $\mathbf{Q}$, plus an error term n:

$$\mathbf{r} = \mathbf{Q}\mathbf{d} + \mathbf{n} \tag{2.18}$$

where $\mathbf{Q}$ is the unknown transformation matrix to be estimated and $\mathbf{n}$ is a residual error vector assumed to have zero mean. In the context of spectral estimation, each column of $\mathbf{d}$ represents the response from one channel and $\mathbf{r}$ contains the full spectral data.

In order to make 2.18 be in the form of 2.12 we will rewrite it in this form:

$$\mathbf{r} = [\mathbf{Q} \;\; \mathbf{n}] \begin{bmatrix} d \\ 1 \end{bmatrix} \tag{2.19}$$

where $\mathbf{Q}$ is a $N \times K$ matrix and $\epsilon$ is a $N \times 1$ vector. The criterion is to minimize the sum of squared error, so we express $\mathbf{Q}^{MLR}$ as

$$\mathbf{Q^{MLR}} = [\mathbf{Qn}] \tag{2.20}$$

we can see that now, $\mathbf{Q}^{MLR}$ is a $N \times (K+1)$ matrix. We also have to define $\mathbf{d}^* = [\mathbf{d} \;\; 1]^T$ which is a $K+1 \times 1$ vector. Now, we can replace $\mathbf{Q}$ with $\mathbf{Q}^{MLR}$

in 2.16 :

$$\arg\min_{\mathbf{Q}} E\{\|\mathbf{r} - \mathbf{Q}^{MLR} {d^*}_m\|^2\}. \tag{2.21}$$

In this method, the **training phase** consists of using a set of reference data-pairs of known camera responses ($\mathbf{d}$) and their corresponding spectral reflectances ($\mathbf{r}$) to compute the optimal transformation matrix $\mathbf{Q}^{MLR}$. This is achieved by minimizing the sum of squared errors between the predicted and actual reflectances over the training set. The result is a matrix $\mathbf{Q}^{MLR}$ (and optionally an intercept vector) that best maps the input camera responses to the output spectra in a least-squares sense.

During the **estimation phase**, this learned matrix $\mathbf{Q}^{MLR}$ is applied to new, unseen camera measurements. The new measurement vector is augmented (typically by appending a 1 to account for the intercept), and the estimated spectrum is obtained by a simple matrix multiplication with $\mathbf{Q}^{MLR}$. This process is computationally efficient and does not require retraining or access to the original training data.

So, the **training phase** determines the optimal linear mapping from camera responses to spectra by learning the matrix $\mathbf{Q}^{MLR}$, while the **estimation phase** uses this matrix to quickly predict spectra from new measurements.

This problem is the same as Wiener with the only difference being in the replacement of $\mathbf{d}$ with $d^*$. After finding the optimal $\mathbf{Q}^{MLR}$ we replace that in 2.18 in order to calculate $\mathbf{r}$.

### 2.4.3 Sparse Dictionary Learning (K-SVD)

In applied mathematics, K-SVD is a dictionary learning algorithm for creating a dictionary for sparse representations, via a singular value decomposition approach. K-SVD is a generalization of the k-means clustering method, and it works by iteratively alternating between sparse coding the input data based on the current dictionary, and updating the atoms in the dictionary to better fit the data. Using this approach we make the assumption that each high-dimensional spectral reflectance vector $\mathbf{r}$ can be well approximated as a sparse linear combination of atoms from a learned dictionary $\mathbf{D}$. In other words, we express each reflectance as

$$\mathbf{r} = \mathbf{DA} \tag{2.22}$$

where $\mathbf{D}$ is a dictionary $p \times k$ matrix($\mathbf{D} = [d_1, d_2, ...d_k]$) with k representing the number of dictionary atoms [29],[30], $\mathbf{A}$ is a $k \times 1$ sparse coefficient vector($\mathbf{A} = [a_1, a_2, .., a_k]$) and p is the number of sampled wavelengths. The sparsity constraint implies that most entries in $\mathbf{A}$ are zero so that only a few atoms are active in representing $\mathbf{r}$.

The goal is to learn both the dictionary $\mathbf{D}$ and the sparse representations $a_i$ from a set of $N$ training spectral reflectance vectors
$\mathbf{R} = [r_{o1}, r_{o2}, ..., r_{on}, r_i \in \mathbb{R}^p]$. This problem is formulated as the following optimization problem :

$$\min_{D,a_i} \sum_{i}^{N} ||\mathbf{R} - \mathbf{DA}||_2^2$$

$$\text{subject to } ||a_i||_0 \leq s, \quad \forall i \in [1, k]$$

where s is the sparsity constrain.

This optimization problem is not convex and solving the problem is NP-hard.

However, with respect to each of the two variables $\mathbf{D}$ or $\mathbf{A}$ when the other one is fixed, the problem becomes convex, but it is not jointly convex in $\mathbf{D}$,$\mathbf{A}$. The problem can be described as a convex optimization problem with respect to either the dictionary or sparse coding so, the K-SVD idea [31] is to update one and then the other. K-SVD consists of two steps:

- For a fixed dictionary D, the sparse coefficients $a_i$ are computed for each training sample $r_i$ using the greedy algorithm Orthogonal Matching Pursuit(OMP), which seeks a sparse solution satisfying the above constraint.

- After the sparse codes are fixed, each atom $d_k$ is updated sequentially. Now we have that

$$\mathbf{r} = \mathbf{D}\mathbf{a}^* \tag{2.23}$$

  where $a^* \in \mathbb{R}$. The coefficient vector $\mathbf{a}^*$ can be optimized as

$$\mathbf{a}^* = (\mathbf{S}^\mathbf{T}\mathbf{D})^{-}\mathbf{d} \tag{2.24}$$

In this method, the **training phase** involves learning both the dictionary matrix $\mathbf{D}$ and the optimal sparse coefficient vectors $\mathbf{a}_i$ for a set of training spectra. This is achieved by alternately optimizing the dictionary atoms and the sparse codes to best reconstruct the training data under a sparsity constraint. The result of the training phase is a dictionary $\mathbf{D}$ whose atoms capture the essential patterns in the spectral data, enabling sparse representations.

During the **estimation phase**, the learned dictionary $\mathbf{D}$ is kept fixed. For a new, unseen measurement (e.g. a set of camera responses or a partial spectrum), the algorithm computes the sparse coefficient vector $\mathbf{a}^*$ that best

reconstructs the measurement using as few dictionary atoms as possible (subject to the sparsity constraint). The estimated spectrum is then obtained by multiplying the dictionary $\mathbf{D}$ by the sparse coefficient vector $\mathbf{a}^*$. This step typically involves solving a sparse coding problem, such as with Orthogonal Matching Pursuit (OMP) or LASSO.

So, the **training phase** learns a dictionary of spectral patterns from the training data, while the **estimation phase** uses this dictionary to represent new measurements as sparse combinations of these patterns, enabling efficient and accurate spectral reconstruction.

The complexity of this method is O(pk), where p is the number of sampled wavelengths and k is the number of atoms. The training phase requires a constant number of multiplications because it takes place only one time.

### 2.4.4 Principal Component Analysis (PCA)

Principal component analysis (PCA) is a technique extensively used for dimensionality reduction in a dataset. It consists of finding an orthogonal basis composed of vectors called principal components. Each component is associated with an energy that indicates the statistical relevance of the vector in the data. Technically speaking, PCA is an orthogonal linear transformation that transforms the data to a new coordinate system such that the greatest variance by any projection of the data lies on the first coordinate (called the first principal component), the second greatest variance on the second coordinate, and so on. In the field of MultiSpectral imaging, PCA has been largely used for data compression but also in spectral reflectance reconstruction.

This method is similar to the Wiener method with the difference being that in this method we approach $\mathbf{r}$ by using the basis matrix $\mathbf{B}$ and the

weight vector $\mathbf{a}$ such that every reflectance $\mathbf{r}$ could be rewritten as :

$$\mathbf{r}=\mathbf{Ba} \tag{2.25}$$

In [7] the same problem is being studied and the solution that is suggested is as follows:

$$\mathbf{d} = \mathbf{S^T Ba} \tag{2.26}$$

where a is $m \times 1$ vector that has all the weights that define the spectrum we are trying to reconstruct. The equation 2.26 can be solved as shown:

$$\mathbf{a} = (\mathbf{S^T B})^{-}\mathbf{d} \tag{2.27}$$

So this means that

$$\mathbf{Q^{PCA}} = \mathbf{B}(\mathbf{S^T B})^{-} \tag{2.28}$$

In this method, the **training phase** involves analyzing a set of reference spectra to compute the principal components, an orthogonal basis that captures the directions of greatest variance in the data. This results in a basis matrix $\mathbf{B}$ (whose columns are the principal components) and a mean spectrum vector. These components are learned from the training data and are fixed after training.

During the **estimation phase**, the learned basis matrix $\mathbf{B}$ is used to reconstruct new spectra from limited measurements (e.g., camera responses). Given a new measurement, the algorithm solves for the weight vector $\mathbf{a}$ that best represents the measurement in the principal component space, typically by solving a least-squares problem. The estimated spectrum is then reconstructed as a linear combination of the principal components, using the computed weights.

Hence, the **training phase** learns the principal components (basis vectors) that capture the main variations in the spectral data, while the **estimation phase** projects new measurements onto this basis to reconstruct the full spectrum efficiently.

### 2.4.5 Probabilistic Principal Component Analysis (PPCA)

Probabilistic Principal Component Analysis (PPCA) is a statistical extension of classical PCA, providing a probabilistic generative model for the observed reflectance spectra [32]. In PPCA, each reflectance vector $r \in \mathbb{R}^N$ is modeled as a linear combination of $M$ latent variables plus Gaussian noise:

$$\mathbf{r} = \mathbf{B}\mathbf{a} + \mu + \mathbf{n} \tag{2.29}$$

where $B$ is an $N \times M$ matrix whose columns are the principal axes (basis vectors), $a \in \mathbb{R}^M$ is a vector of latent variables (coefficients),$\mu$ is the mean reflectance vector,$n \sim \mathcal{N}(0, \sigma^2 I_N)$ is Gaussian noise.

The observed camera outputs $d$ are related to the reflectance $r$ via the linear model (as in Eq. 2.17):

$$\mathbf{d} = \mathbf{S}\mathbf{r} + \mathbf{n} \tag{2.30}$$

where $\mathbf{S}$ is the $K \times N$ matrix of camera spectral sensitivities, and $\mathbf{n}$ is a noise vector.

Given a set of measured camera outputs $\mathbf{d}$, the goal is to estimate the reflectance $\mathbf{r}$. In the PPCA framework, this is done by first estimating the latent variables $\mathbf{a}$ that best explain the observed $\mathbf{d}$, and then reconstructing $\mathbf{r}$ as $\mathbf{r} = \mathbf{B}\mathbf{a} + \mu$.

The estimation of $\mathbf{a}$ is typically performed by minimizing the following regularized least squares problem:

$$\mathbf{a} = \arg\min_{a} \|\mathbf{d} - \mathbf{S}(\mathbf{B}\mathbf{a} + \mu)\|^2 + \lambda\|\mathbf{a}\|^2 \tag{2.31}$$

where $\lambda$ is a regularization parameter related to the noise variance $\sigma^2$.

The solution for $\mathbf{a}$ is given by:

$$\mathbf{a} = \left((\mathbf{SB})^{\mathbf{T}}\mathbf{SB} + \lambda I\right)^{-1} (\mathbf{SB})^{\mathbf{T}}(\mathbf{d} - \mathbf{S}\mu) \tag{2.32}$$

The estimated reflectance is then:

$$\hat{\mathbf{r}} = \mathbf{Q}^{\mathrm{PPCA}}\mathbf{d} + \mu \tag{2.33}$$

where the operator $Q^{\mathrm{PPCA}}$ is defined as:

$$\mathbf{Q}^{\mathrm{PPCA}} = \mathbf{B}\left((\mathbf{SB})^{\mathbf{T}}\mathbf{SB} + \lambda\mathbf{I}\right)^{-1} (\mathbf{SB})^{\mathbf{T}} \tag{2.34}$$

This operator $Q^{\mathrm{PPCA}}$ maps the measured camera outputs $\mathbf{d}$ to the estimated reflectance $\hat{\mathbf{r}}$ in the PPCA framework, incorporating both the learned basis and the regularization due to noise. PPCA models the reflectance as a linear combination of basis vectors plus Gaussian noise, providing a probabilistic interpretation of PCA. The principal axes (columns of $\mathbf{B}$) are analogous to the principal components in classical PCA. In this work, the Factor Analysis algorithm is used as a practical implementation of PPCA, which estimates both the principal components and the noise variance from the training data.

In this method, the **training phase** involves fitting a probabilistic model to a set of reference spectra. This process estimates the principal axes (basis matrix $\mathbf{B}$), the mean spectrum vector ($\mu$), and the noise variance ($\sigma^2$). These parameters are learned from the training data, using Factor Analysis, and are fixed after training.

During the **estimation phase**, the learned parameters ($\mathbf{B}$, $\mu$, and $\sigma^2$) are used to reconstruct new spectra from limited measurements (e.g., camera responses). Given a new measurement, the algorithm solves a regularized least-squares problem to estimate the latent variable vector $\mathbf{a}$ that best explains the observed data, taking into account both the basis and the noise model. The estimated spectrum is then reconstructed as a linear combination of the principal axes plus the mean, using the computed weights.

So, the **training phase** learns the principal axes, mean, and noise characteristics of the spectral data, while the **estimation phase** uses these learned parameters to infer the most probable spectrum for new measurements, providing a probabilistic interpretation and regularization that improves robustness to noise.

# Chapter 3

# Experiments

## 3.1 Training and Estimation Data

Two different experiments will take place. In the first Macbeth Color Checker will be used for the evaluation of the models and Photos from natural objects will be used for testing. In the Second experiment Macbeth Color Checker will be used for testing of the models and Photos from natural objects will be used for the evaluation.

### 3.1.1 Macbeth Color Checker

Specifically engineered for the demands of digital imaging professionals, the Digital ColorChecker SG features the finest color benchmarks on the market. Its 140 precisely selected swatches span a wide expanse of color space, enabling you to build profiles that harness your camera's and scanner's full potential.

This SG version retains all of the classic ColorChecker hues-many drawn from real-world elements like skin tones, foliage, and clear skies-while adding extra patches for a broader range of complexions. A graduated gray scale ensures your camera's balance stays perfectly neutral under any light, and you can even use it to set an exact white balance in-camera, ensuring uniform,

true-white rendering across all lighting conditions.

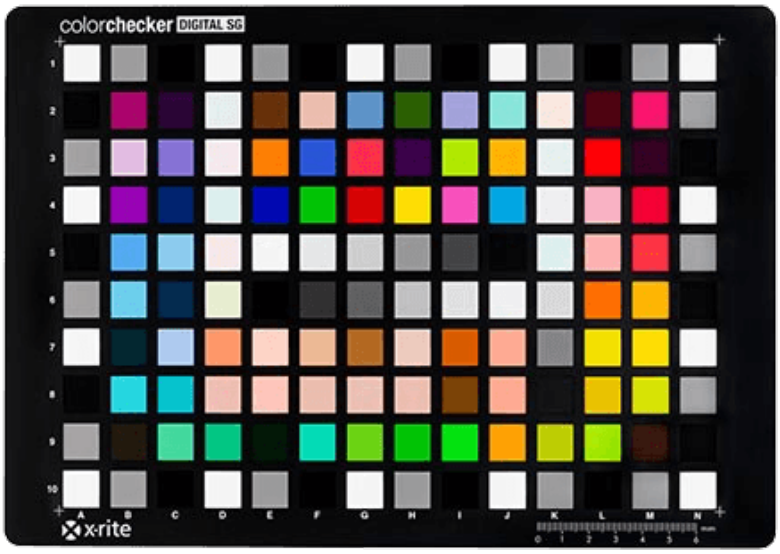


Figure 3.1: Macbeth Color Checker([8])

### 3.1.2 Spectral dataset of natural objects' reflectance from the Southern cone of South America

This dataset currently contains the spectral reflectance of 532 samples of natural objects, ranging from 400 to 1000 nm in 4 nm increments. These records correspond to plants (302 samples), animals (167 samples), and stones (63 samples). The objects were collected in the field, purchased at local fruit and vegetable markets, or borrowed from museum collections in San Miguel de Tucuman, Argentina [33].

In order for this dataset to be used a pre-process took place. First of all only the data from 400 to 1000 nm was kept and due to the fact that the data which got tested was from 400 with 5 nm increments a matching process took place. The closest wavelength from the training set which has a 4nm increment was matched with the given wavelength from the test data. So if 464 nm from the training set was matched with 465 468 with 470 and so on.

## 3.2 Hardware Used

The Spectra of Macbeth ColorChecker was acquired using the MUSES9-HS, which is a powerful full frame, tunable filter-based HyperSpectral imager, used for spectroscopy and spectrometry. It has a wide spectral range from 370 nm (UV) to 1000 nm (NI) and is able to acquire 126 spectral images with a step of 5 nm in about 40 seconds. From those images millions of spectra can be extracted and used by a graphical user interface. This imager has a 6.4 Megapixel spatial resolution and the spectral resolution ranges from 7 nm for visible or NIR to 18 for visible and NIR.

Due to the fact that the camera has an acquisition integral of 10 nm, in contrast with the spectrometer that has lower than 1nm, a pre-process of the data must take place. In order for our data to be usable and not create unnecessary errors we have to make a smoothing process first. Also it must be ensured that the produced spectral cube is aligned.

The most important thing that MUSES9-HS provides is the fact that it has all the devices needed for the acquisition of the spectra compacted in one camera. That eliminates the difficulty of muliple-device calibration process and the risk of a false aligning that would produce noise or error. In sort terms, MUSES9-HS makes the work for this study a lot easier.

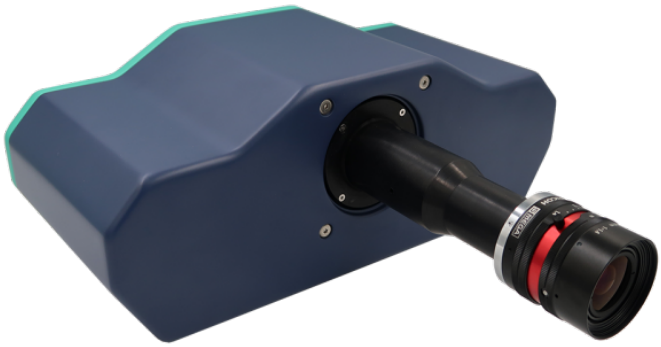

Figure 3.2: MUSES9-HS Camera[9]

The training set was the Spectral dataset of natural objects' reflectances and the testing was conducted using the Macbeth Color Checker.

## 3.3 Training

This study will focus on the visible and NIR spectrum [400nm-1000nm]. In order for the experiments to be easier, a graphical user interface was designed. The software uses Qt libraries and provide the user with the following:

- Begins with a spectral cube loaded but another one can also be loaded dynamically
- Dynamic choice of specific target pixel by hovering the mouse
- Dynamic selection of estimation method
- Real time visualization of selected spectrum
- Real time visualization of spectral estimation
- Real time calculation of error metric
- Dynamic selection of sample bands
- Real time analysis for a specific method for all the squares of Macbeth board
- RMSE heatmap of the board
- Real time calculation of RMSE using different sample bands starting from 121 to 7 with step 5 until 20 bands and 1 step after
- Plot of the RMSE compared to the sample bands
- Scoring of all the algorithms

- Producing the comparison of original and estimated spectra and the original and estimated color chart.

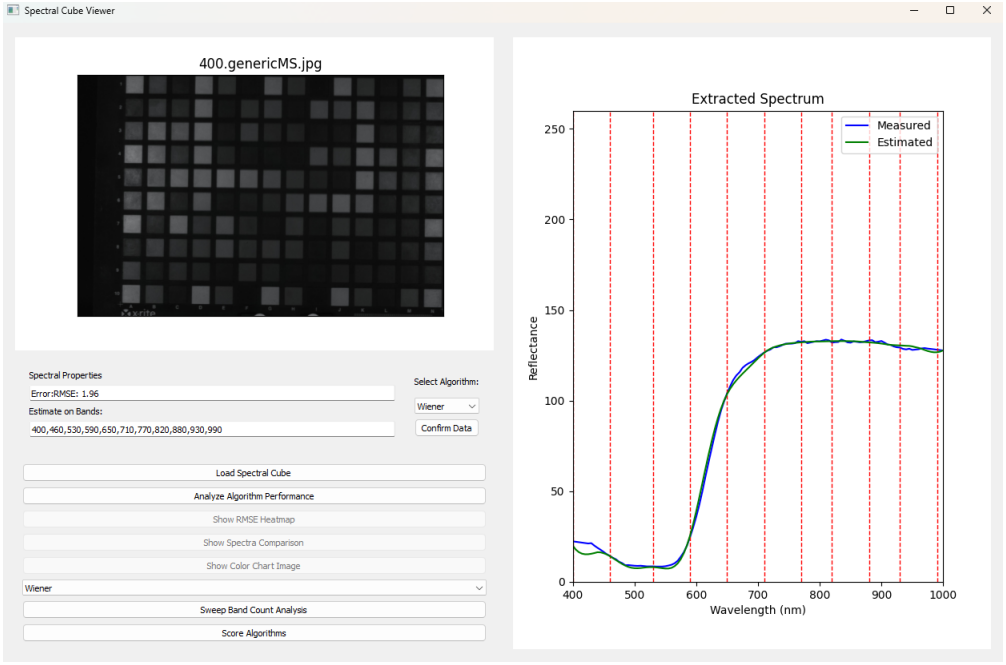


Figure 3.3: Application Example 1

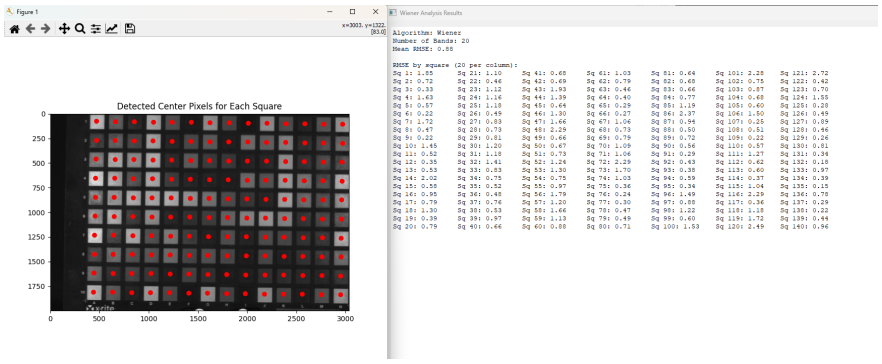


Figure 3.4: Application Example 2

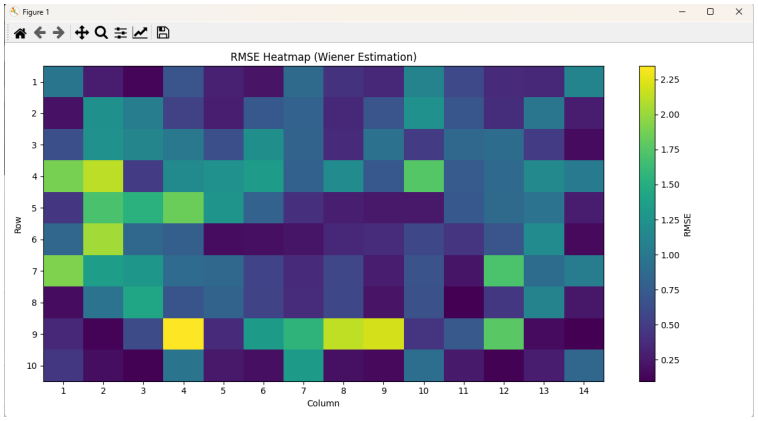


Figure 3.5: Application Example 3

### 3.3.1 Parameter Tuning

In this section the hyper-parameters of each method will be presented.

- Wiener method could work for $\gamma = 0$ but because the data may not be ideal the noise parameter was chosen to be $\gamma = 10^{-5}$.
- PCA method depends on the number of the eigenvectors for it's accuracy. Increasing the number of the eigenvectors increases accuracy until a limit that achieves over 99.9% accuracy and further up from that doesn't make a difference. In this research the number of eigenvectors was set to 10.
- In PPCA method the number of latent factors/components was set to 20.
- The noise of linear Regression method was set to 0.
- The number of atoms in Dictionary learning was set to 100.

## 3.4 Experiment 1

### 3.4.1 Testing

In the first Experiment Macbeth Color Checker was used for evaluation and images from natural objects were used for training. In testing each algorithm will be performing estimations using from 121 to 7 bands with a step of 5 nm from 121-20 and then 1 nm step until 7 for better precision. The thing that we try to see is whether the algorithm is accurate even with smaller amount of sample bands and which are the breakpoints of each algorithm performance. In the following section we will analyze that breakpoints and score the algorithms based on them and also the time they need to estimate. The results for each algorithm are the following:

#### Wiener

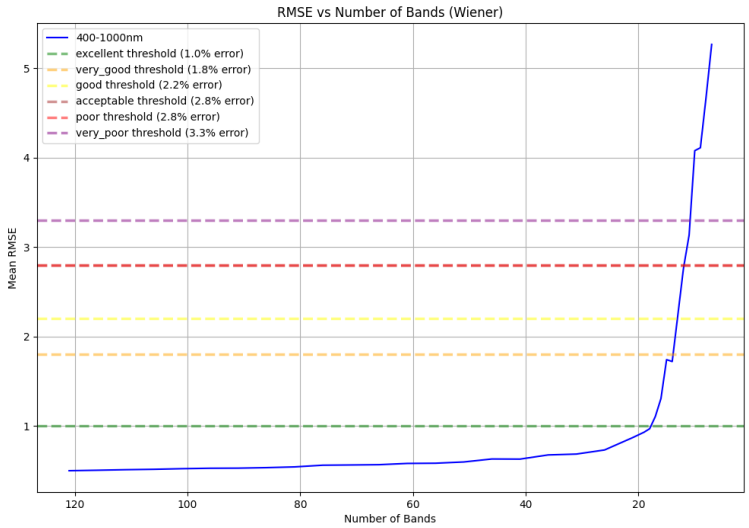


Figure 3.6: Wiener Results

We also present a comparison image of the original spectra with the estimated spectra and the RMSE heatmap it has. For all the algorithms 10 sample bands where used to present the original 121 bands. Also the original

and the estimated images are presented.

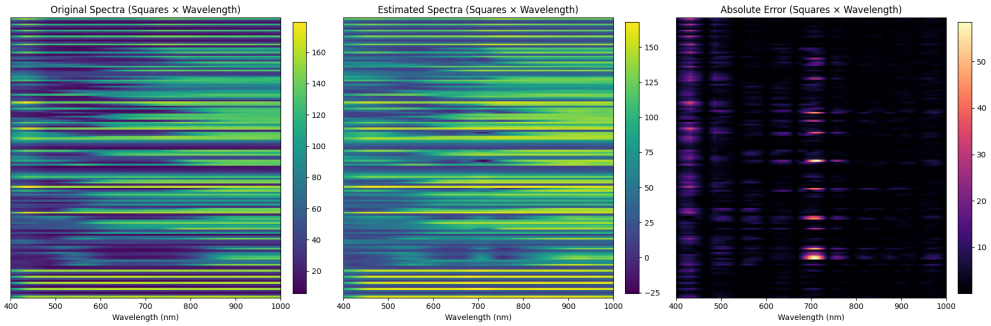


Figure 3.7: Wiener comparison of spectra

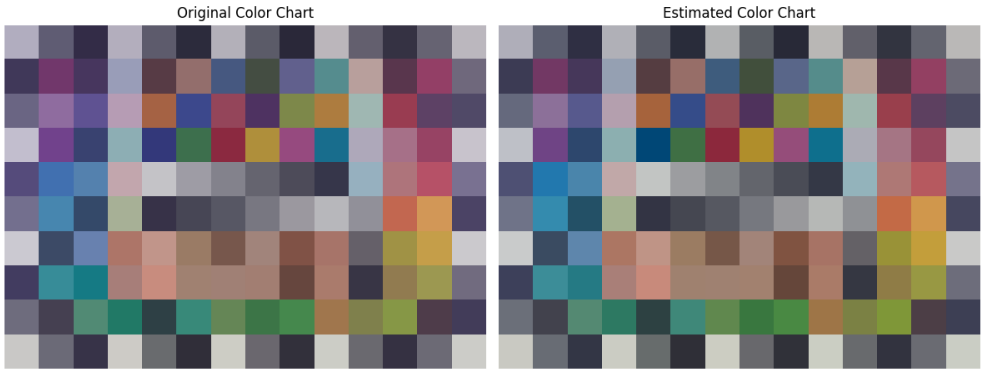


Figure 3.8: Wiener Color Chart

# PCA

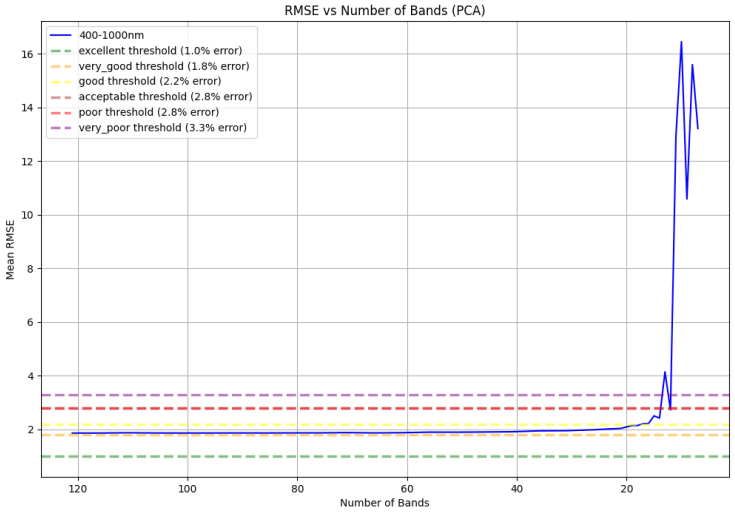


Figure 3.9: PCA Results

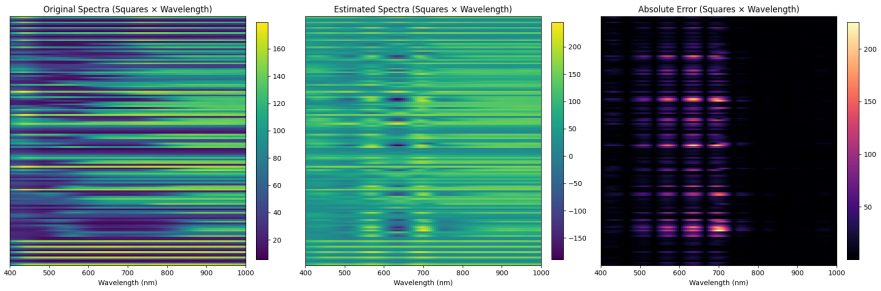


Figure 3.10: PCA comparison of spectra

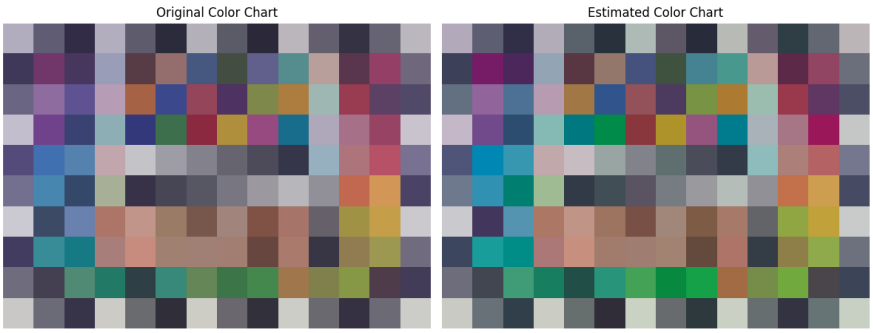


Figure 3.11: PCA Color Chart

# PPCA

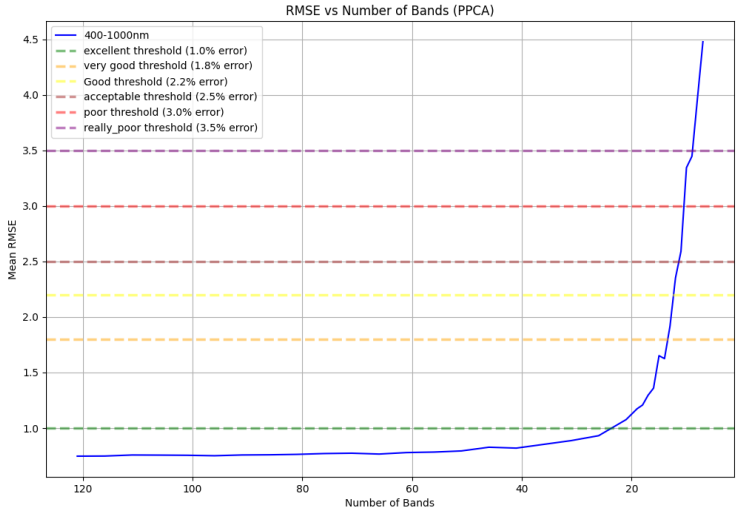


Figure 3.12: PPCA Results

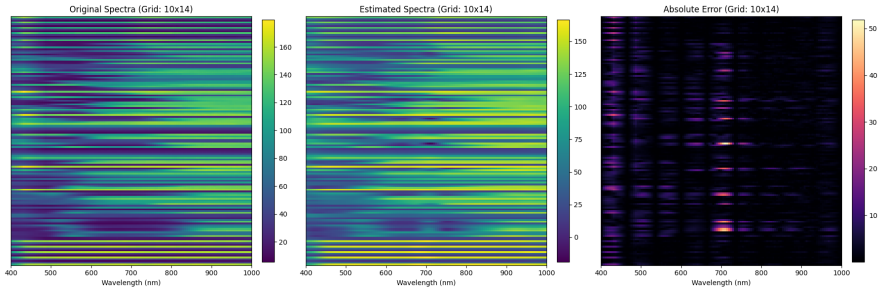


Figure 3.13: PPCA comparison of spectra

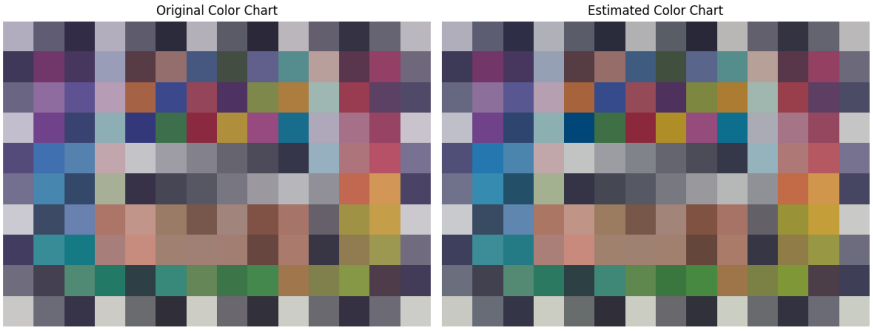


Figure 3.14: PPCA Color Chart

# MLR

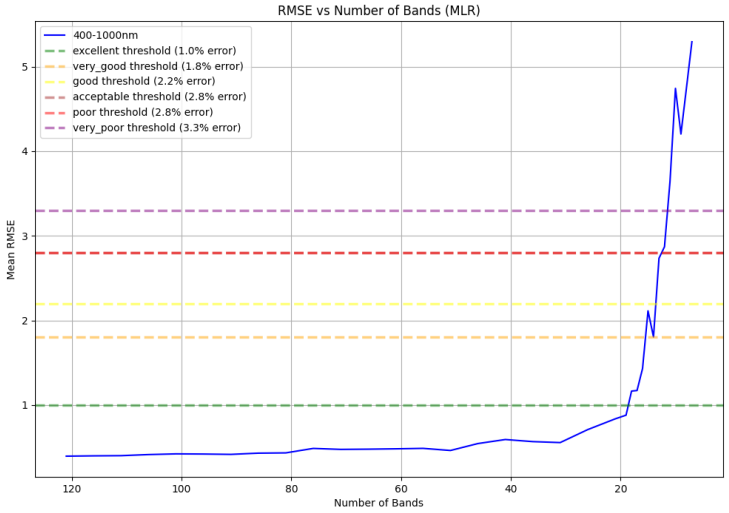


Figure 3.15: MLR Results

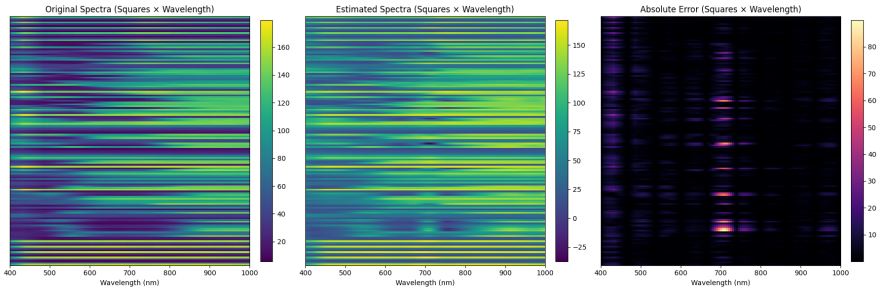


Figure 3.16: MLR Comparison of spectra

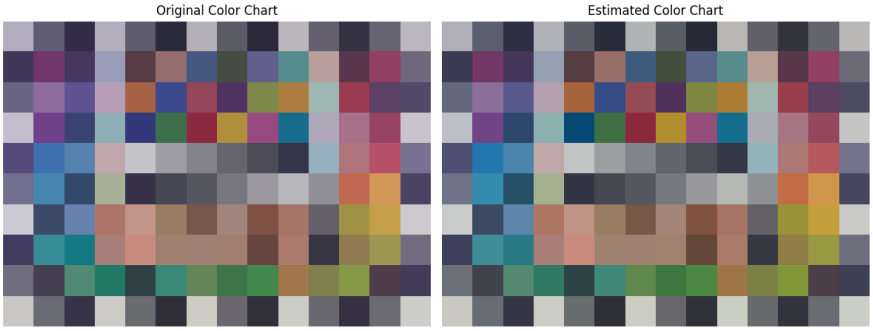


Figure 3.17: MLR Color Chart

# Dictionary Learning

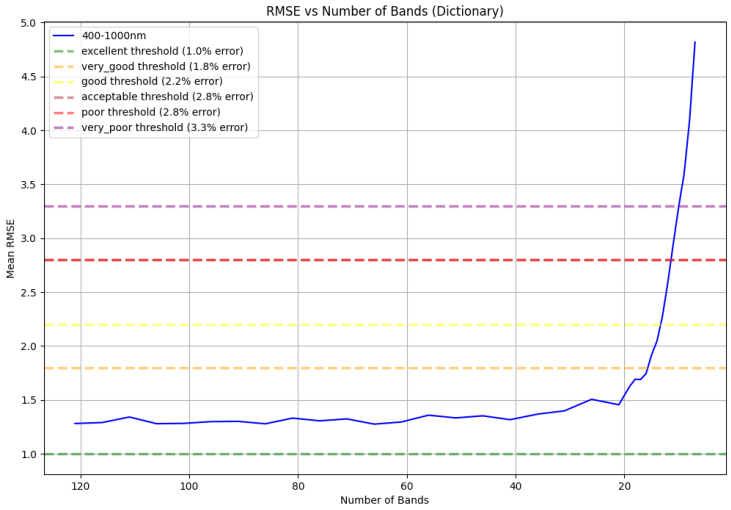


Figure 3.18: Dictionary Learning Results

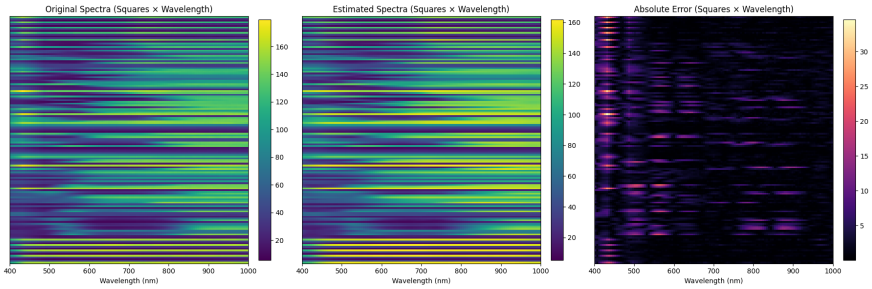


Figure 3.19: Dictionary Learning Comparison of spectra

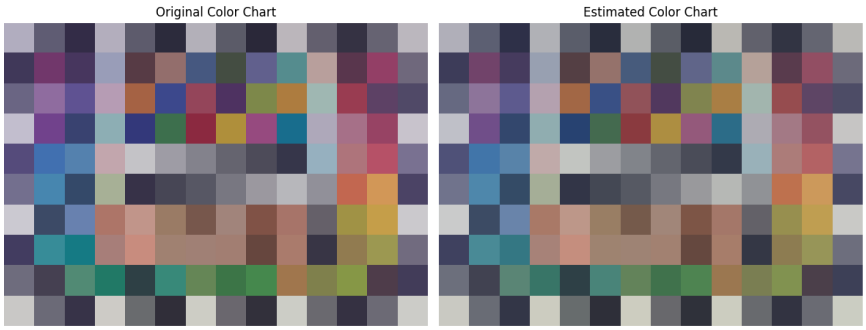


Figure 3.20: Dictionary Learning Color Chart

### 3.4.2 Evaluation

The aim of the experiments is to find whether the number of sample bands is important and, if so, to find the necessary number of bands for the estimation to be considered accurate.

In order for the accuracy of each algorithm to be properly measured some thresholds needs to be determined. RMSE was chosen as the quality indicator because we are interested in spectra. For that reason the following thresholds that are based on RMSE between the estimated and the reference spectra were used.

| **RMSE Value** | **Quality of Estimation** |
|---|---|
| $RMSE \leq 1.0\%$ | Excellent Estimation |
| $1.0\% < RMSE \leq 1.8\%$ | Very Good Estimation |
| $1.8\% < RMSE \leq 2.2\%$ | Good Estimation |
| $2.2\% < RMSE \leq 2.8\%$ | Acceptable Estimation |
| $2.8\% < RMSE \leq 3.3\%$ | Poor Estimation |
| $3.3\% < RMSE$ | Really Poor Estimation |

Table 3.1: RMSE-based Quality of Estimation

There thresholds are really tight. The reason for that is that an excellent estimation must be almost identical to the original spectrum. This is essential for finding the minimum amount of bands needed to score an excellent estimation.

### 3.4.3 Algorithms scoring

The scoring of the algorithms depends on the minimum amount of bands required in order to reach every estimation criterion and the time complexity. In order for an algorithm to be well scored it should have few required bands and a small computational time. Weights were given for the amount of bands and also for the time needed. Because in this thesis time consumption is important, a relatively large weight was given to the time. The weights are

70% for the amount of bands required and 30% for the time needed. Some thresholds based on the bands and the time was set in order for the algorithms to be evaluated. So the thresholds are as follows:

| **Quality of Algorithm** | **Bands required** | **Points Given** |
|---|---|---|
| Excellent | 75 | 100 |
| Very Good | 85 | 80 |
| Good | 95 | 60 |
| Acceptable | 105 | 40 |
| Poor | 115 | 20 |
| Very Poor | 125 | 0 |

Table 3.2: Quality of Algorithm, Bands required and Points Given

| **Quality of Algorithm** | **Time Needed(ms)** | **Points Given** |
|---|---|---|
| Excellent | 1 | 100 |
| Very Good | 2 | 80 |
| Good | 3 | 60 |
| Acceptable | 4 | 40 |
| Poor | 5 | 20 |
| Very Poor | 6 | 0 |

Table 3.3: Quality of Algorithm, Time Needed and Points Given

The algorithm is characterized based on the following formula:

$$Score = (\text{Points from bands}) * 0.7 + (\text{Points from time}) * 0.3$$

Also, if an algorithm fails to reach a quality criterion, a penalty is given so the number bands needed is increased.

| Quality Criterion not reached | Bands added |
|---|---|
| Excellent | 35 |
| Very Good | 40 |
| Good | 45 |
| Acceptable | 50 |
| Poor | -5 |
| Really Poor | -15 |

Table 3.4: RMSE-based Quality of Estimation

These are the scores for the algorithms:

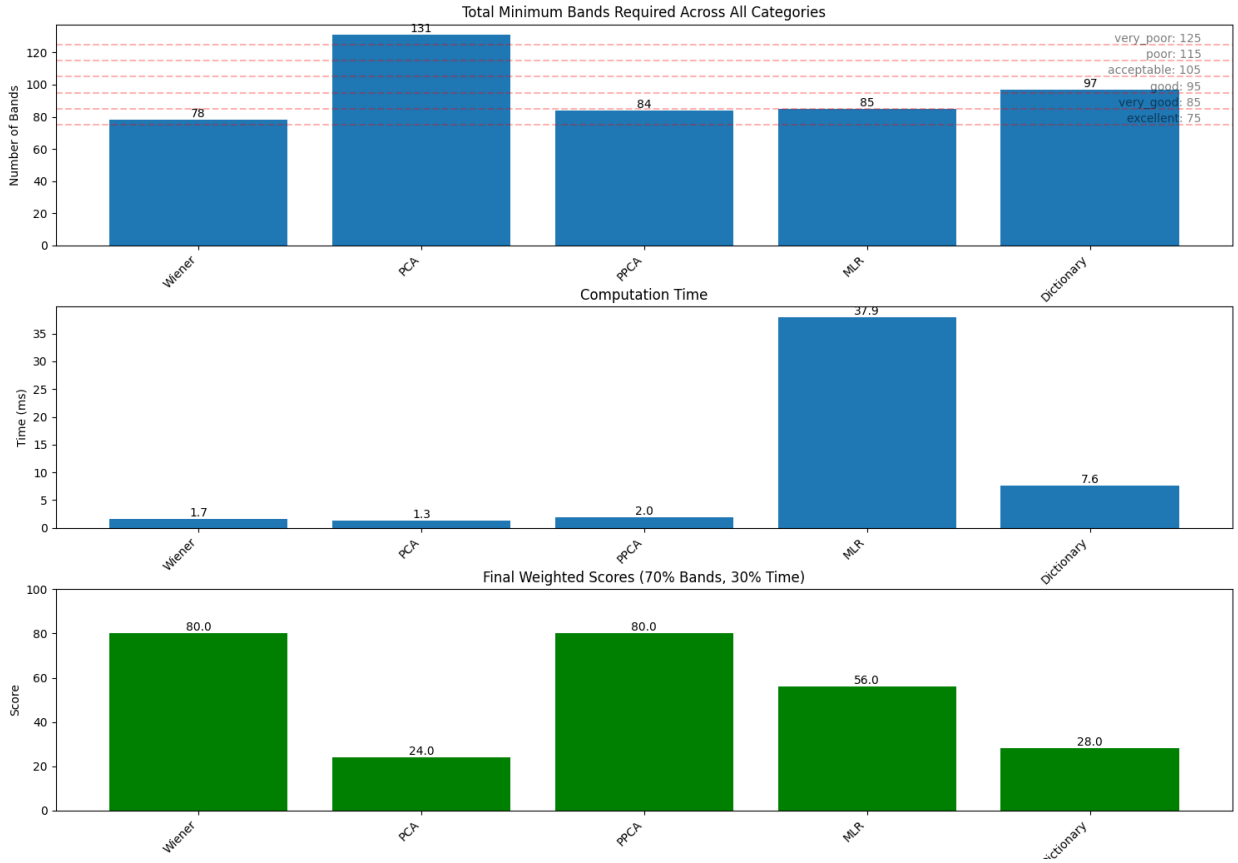


Figure 3.21: Algorithms Scores

Here, the total results for each algorithm will be presented so we can have a better view of how well each algorithm estimates and how consistent it can be.

| Quality | Wiener | PCA | PPCA | MLR | Dictionary |
|---|---|---|---|---|---|
| Excellent | 18 | not reached | 26 | 19 | not reached |
| Very Good | 14 | not reached | 14 | 16 | 16 |
| Good | 13 | 18 | 13 | 14 | 14 |
| Acceptable | 12 | 12 | 11 | 13 | 12 |
| Poor | 11 | 13 | 10 | 12 | 11 |
| Really Poor | 10 | 13 | 10 | 11 | 9 |

Table 3.5: Score of all algorithms

As we see PCA and Dictionary Learning didn't manage to achieve excellent estimation so 35 bands were added to their total score as a penalty as well as 40 points added to PCA for not reaching Very Good estimation.

### 3.4.4 Discussion about Results

By looking at the scores of the algorithms but also at the bands needed and the time consumed for each one of them some very interesting things can be noted.

- First of all it is very important to see that all the algorithms, except MLR, work within a very short amount of time.
- Dictionary Learning seems to be the most consistent algorithm being around 1.3% RMSE until 18 sample bands.
- PPCA is an improvement over PCA because it uses more components(20 compared to 10) and achieves a really good performance without producing any spikes.
- Wiener and PPCA methods perform best, having a really low amount of bands needed to make good estimations and also running in very short time.
- Linear Regression has the third lowest required number of bands, but drops in scoring due to the very long computation time.

- From the comparison images, we observe that all the algorithms seem to struggle to estimate, some specific wavelengths (400-460nm and 680-730nm). The RMSE is increased in those wavelengths which implies the existence of features (valleys or spikes). In general those features are harder to estimate.

Another interesting thing to note is the reason why PCA seems to have a spike in the RMSE when the number of the sample bands approaches the number of the Principal Components that are used as can be seen in 3.9.

In this method, there is a trade-off that has to be taken into account. As we increase the number of principal components that the algorithm runs, we decrease the RMSE value for all the different values of sampled bands until about 5 to 10 more than the number of components themselves. For example, if the number of components is set to 10, the mean RMSE for all the bands from 121 to 14 is about 1.3 and then we see the spikes. If we set the number of components to 20, the mean RMSE is about 0.6 from 121 to 30, but then the spikes appear. So we have to choose the number of components based on the number of sample bands we want to work with. In this thesis, we set that number equal to 10 in order to be able to go pretty low on the number of sampled band used until the RMSE starts to spike, but also get a relatively good estimation.

Spikes happen because when the number of sample bands drop significantly, especially close to or below the number of principal components (which is 10 in this case), the linear system used for reconstruction becomes ill-conditioned. This means there isn't enough information from the few band measurements to reliably determine the principal component coefficients, leading to large errors in the reconstructed spectrum and thus a sharp increase in the Mean RMSE.

We can also observe that MLR method is taking a huge amount of time to estimate the spectrum compared to the other methods. This is due to the fact that the training file of MLR is way bigger in size than all the other

training files of the other methods. The approximate sizes are shown below:

```
File : spectral_wiener_model.pkl
File Size in Bytes: 96797
File : spectral_pca_model.pkl
File Size in Bytes: 10450
File : spectral_ppca_model.pkl
File Size in Bytes: 10528
File : spectral_mlr_model.pkl
File Size in Bytes: 5504754
File : spectral_dict_model.pkl
File Size in Bytes: 88918
```

Figure 3.22: Training file sizes

This is because, the MLR algorithm model is trained for every spectra from 400nm to 1000nm with a 5 nm step. In this version of MLR that has been implemented, the model is trained with a separate regression model for each possible set of input bands (wavelengths). The model learns a matrix Q and intercepts for a specific set of input wavelengths. If the input is changed, the relationship between those inputs and the full spectrum changes, so the learned coefficients Q are no longer valid. The difference with the other methods is that all others learn a basis (PCA, Dictionary), or a statistical model of the spectra (Wiener, PPCA).

If the training files can be cached in the memory of the program, things change significantly.

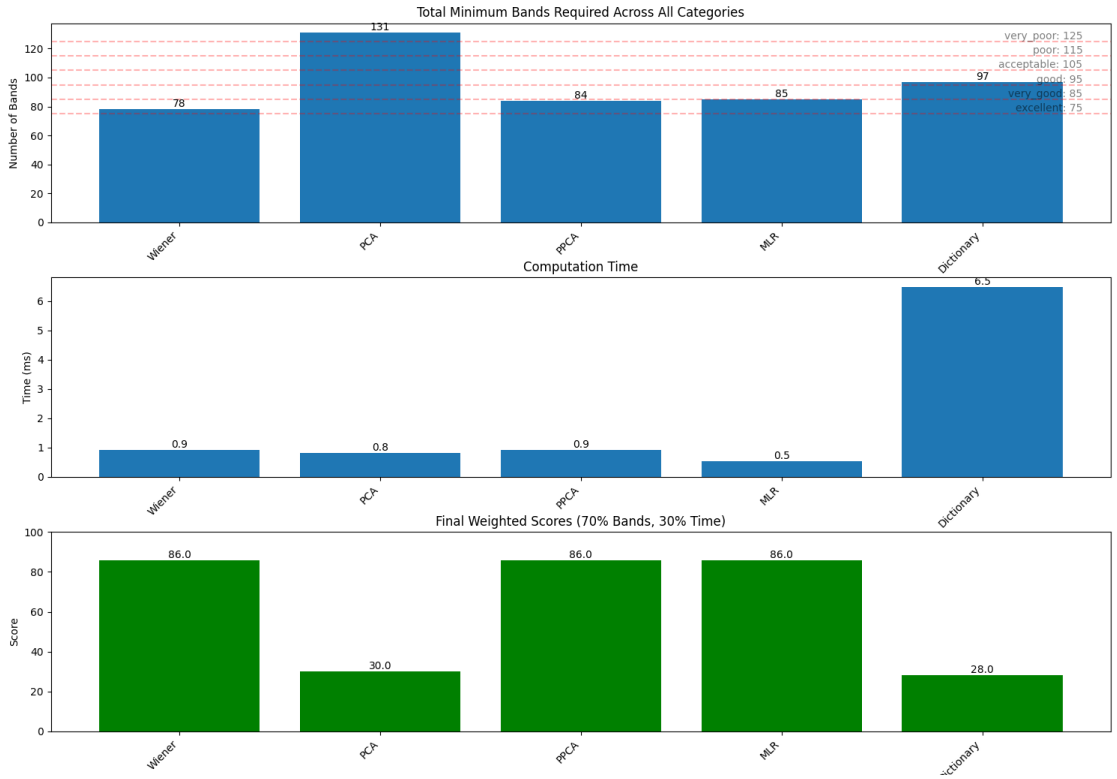


Figure 3.23: Score Results with Cache

As it can be seen here, the results are very different. With a cached file the MLR algorithm performs as well as Wiener and it actually reaches lower RMSE so it can be consider better. Below the lowest RMSE each algorithm achieved is presented.

| **Method** | **Minimum RMSE** |
|---|---|
| Wiener | 0.502 |
| PCA | 1.861 |
| PPCA | 0.747 |
| MLR | 0.396 |
| Dictionary | 1.275 |

Table 3.6: Minimum RMSE values for various spectral reconstruction methods

So to conclude, if the application can not hold cache memory for the trained models, Wiener or PPCA are the best option. If cache memory can be used, MLR is the better choice because it uses the same time as the others

while achieving lower RMSE compared to the other algorithms.

## 3.5 Experiment 2

### 3.5.1 Testing

In the second Experiment Macbeth Color Checker was used for training and images from natural objects for evaluation.

In testing we will try to see how each algorithm performs estimations using again bands from 121 to 7 with a 5 nm step, from 121-20 and then 1 nm step until 7 bands, for better precision.

Again we tried to see whether the algorithm is accurate even with smaller amount of sample bands and try to see which are the breakpoints of each algorithm. Also, we will get a better idea about how the algorithms perform when they are tested in real life objects which don't have so calibrated and accurate spectra as the Macbeth color checker which was used for the testing in the previous experiment.

The results for each algorithm are the following:

# Wiener

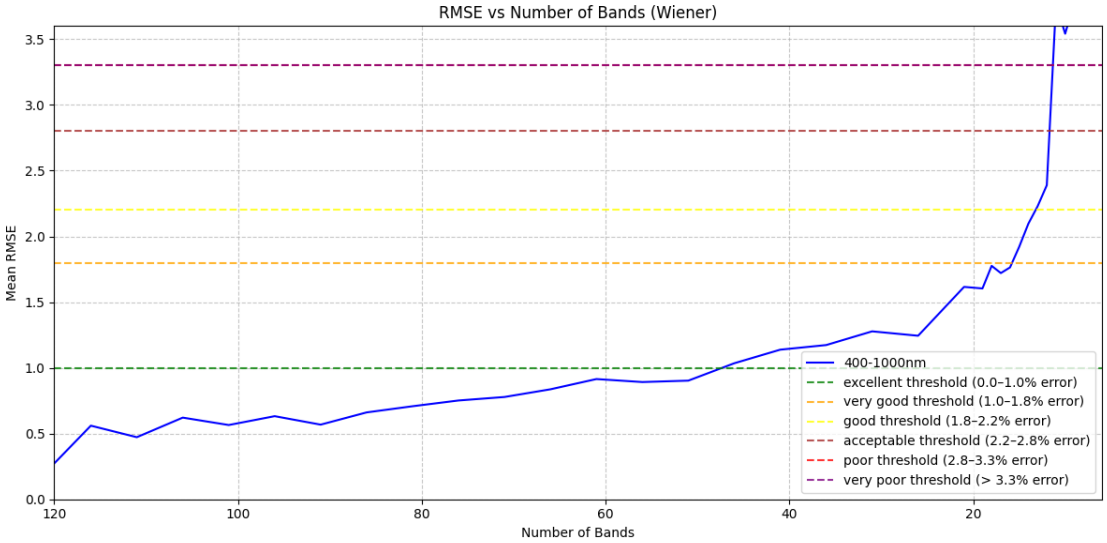


Figure 3.24: Wiener Results

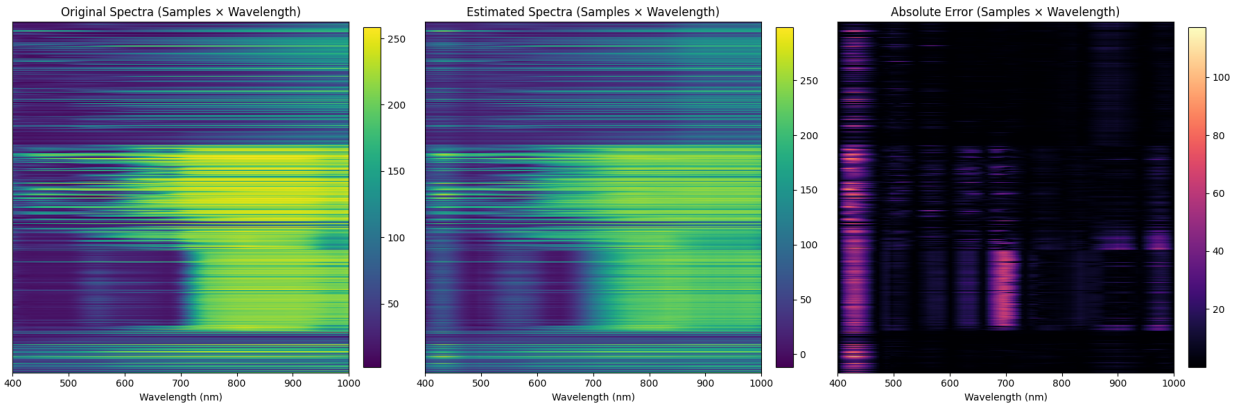


Figure 3.25: Wiener spectra comparison

# PCA

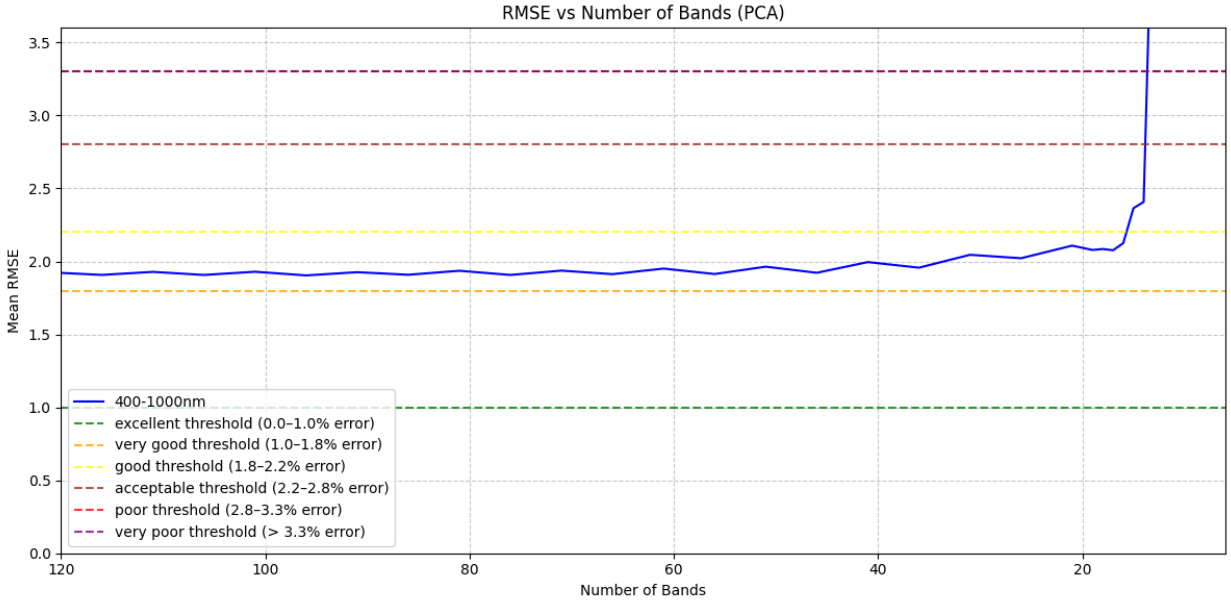


Figure 3.26: PCA Results

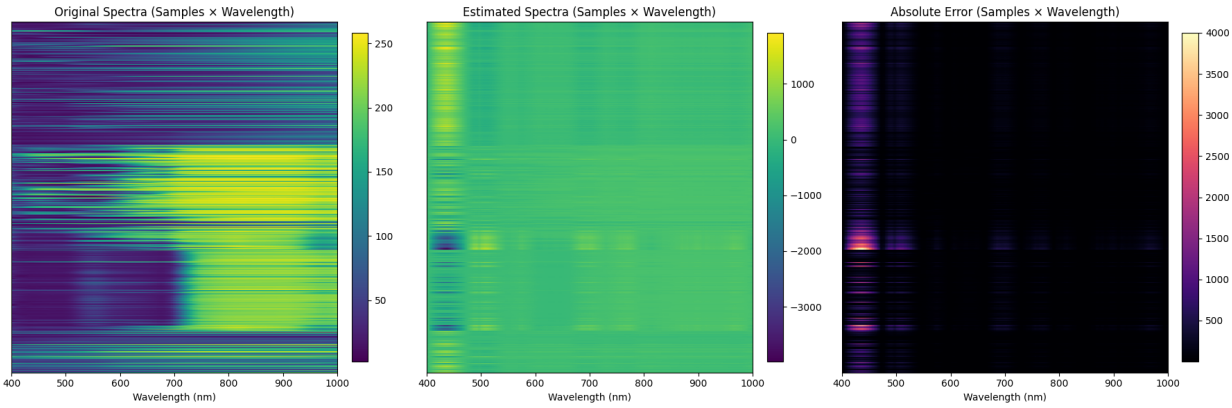


Figure 3.27: PCA spectra comparison

# PPCA

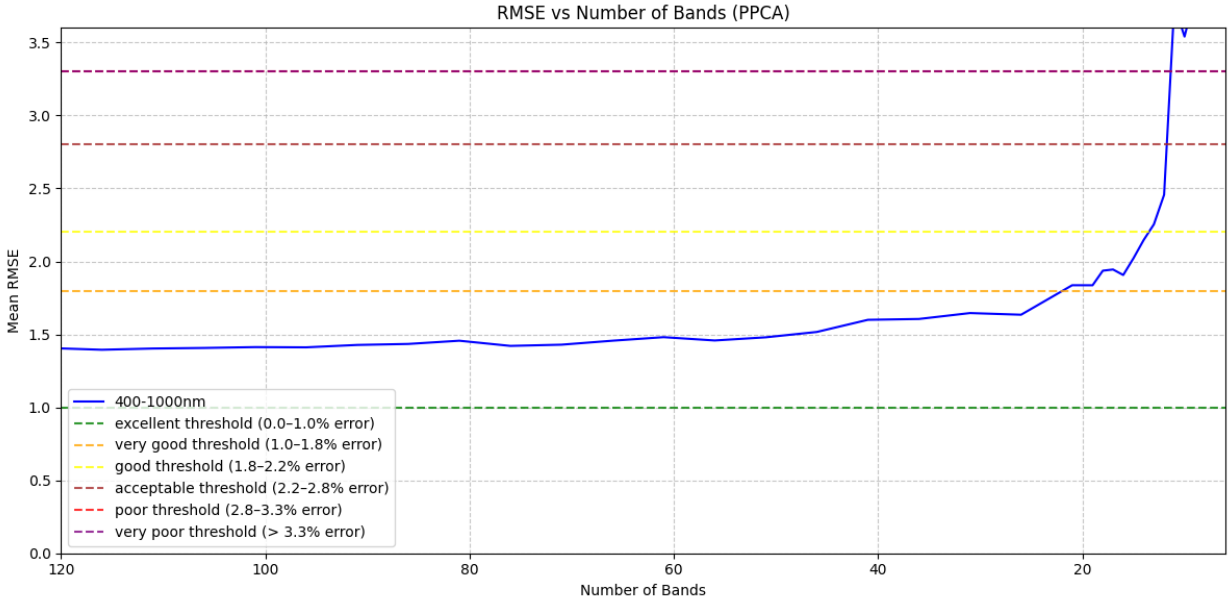


Figure 3.28: PPCA Results

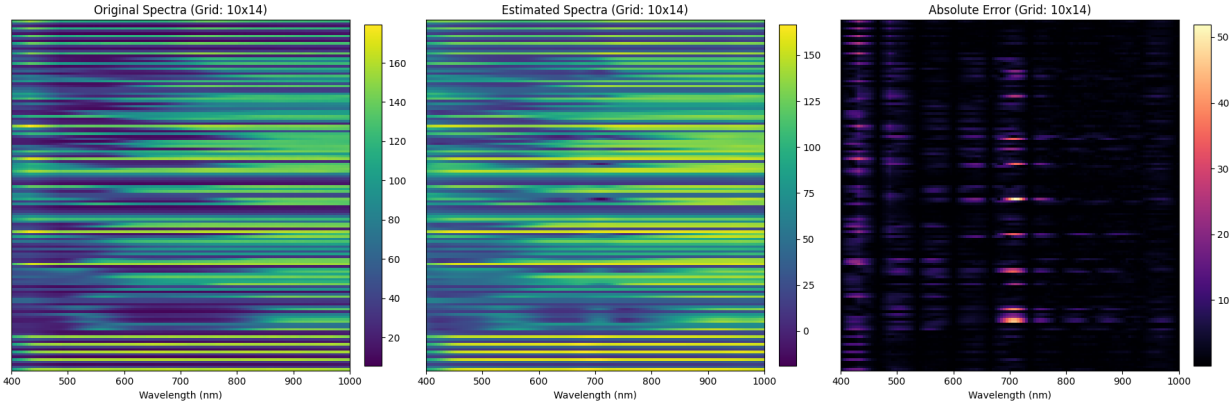


Figure 3.29: PPCA spectra comparison

# MLR

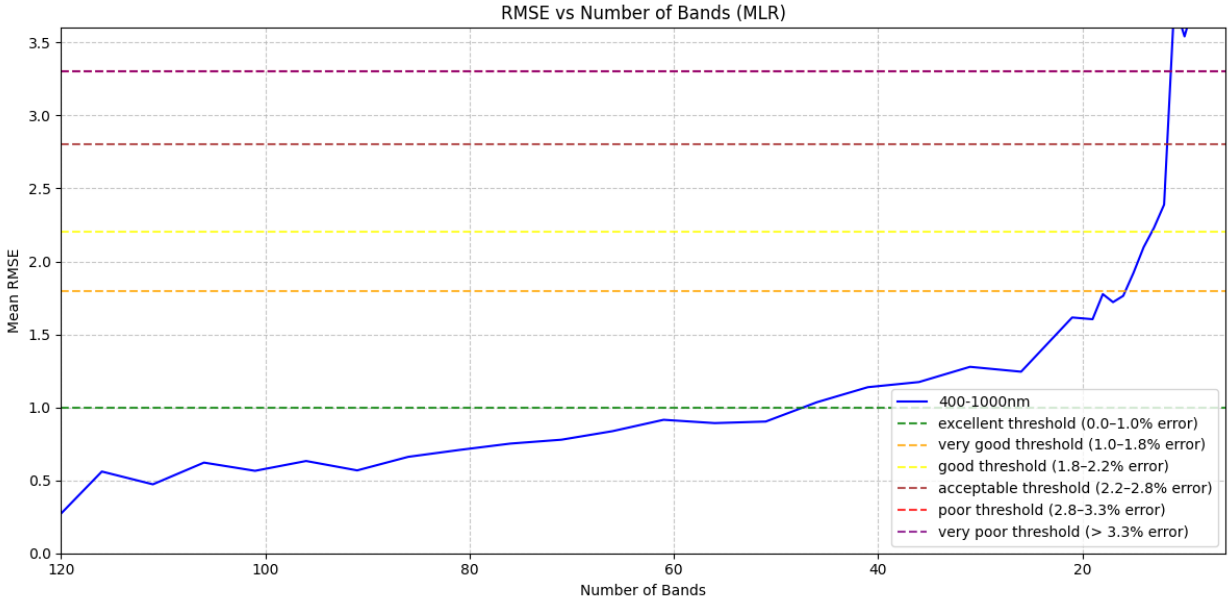


Figure 3.30: MLR Results

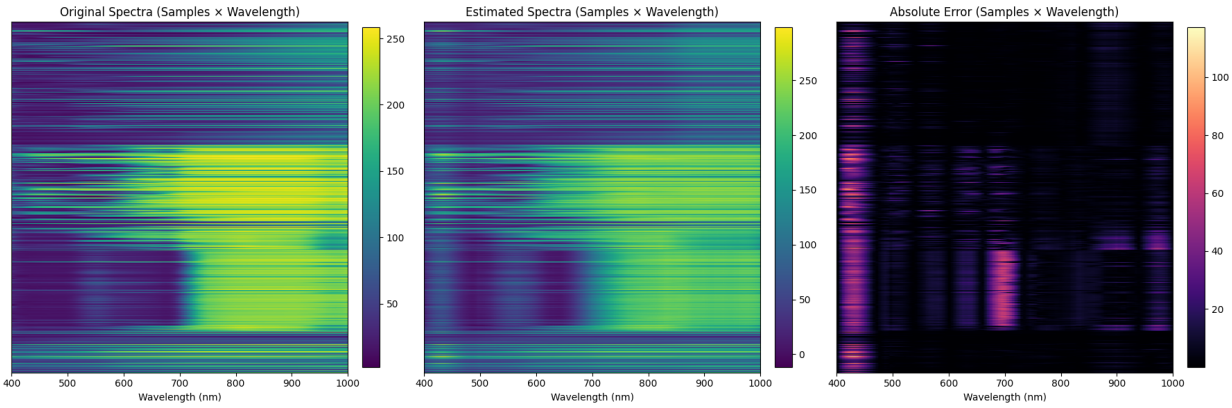


Figure 3.31: MLR spectra comparison

# Dictionary

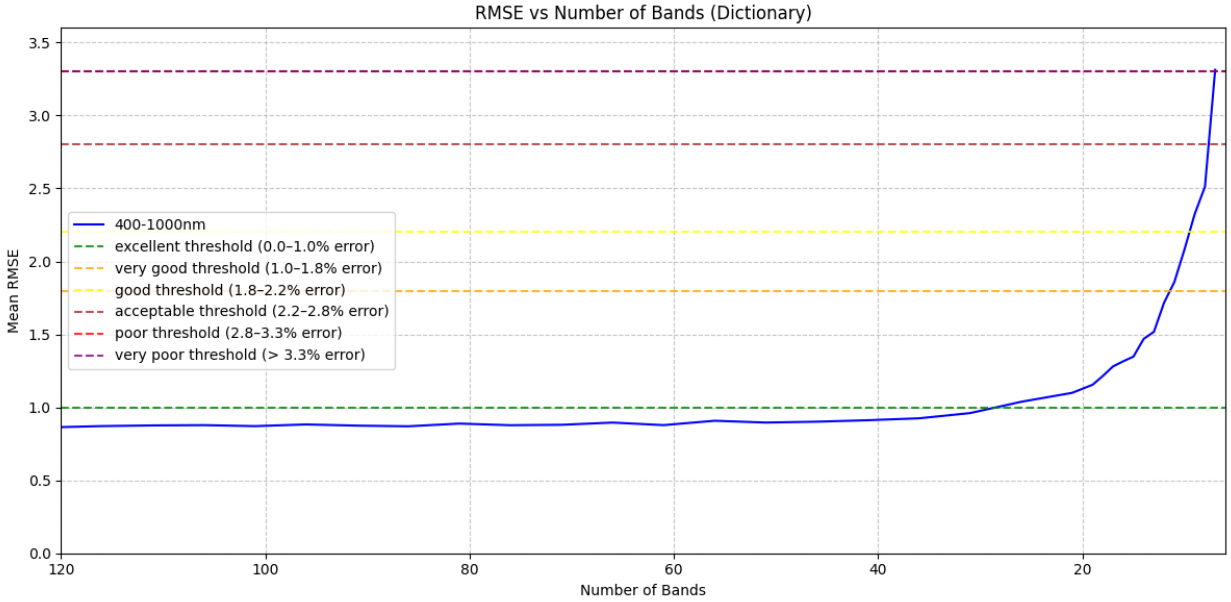


Figure 3.32: Dictionary Results

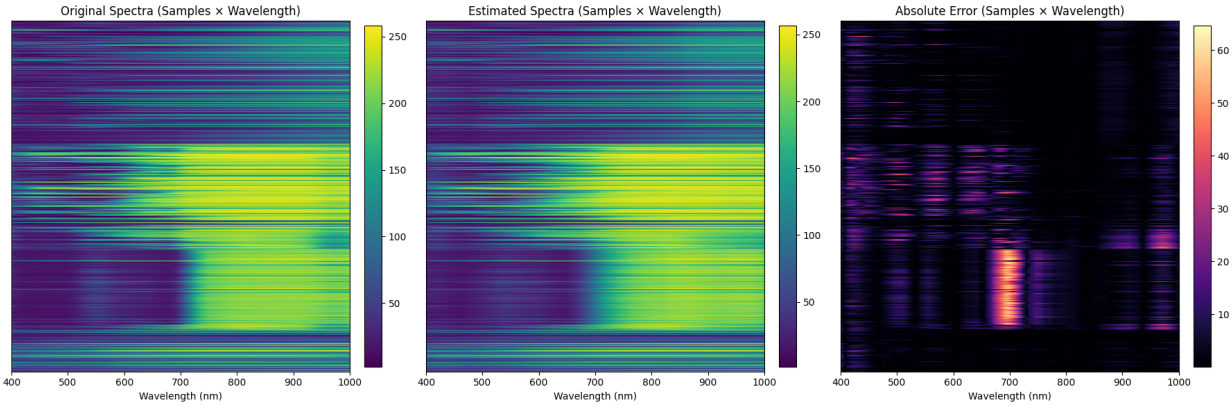


Figure 3.33: Dictionary spectra comparison

### 3.5.2 Evaluation

Again, we will try to find how the number of sample bands affects the performance and the accuracy of our algorithms and try to obtain the necessary number of bands for each algorithm in order for their estimation to be considered accurate.

The same thresholds as in table 3.1 were used in order to determine the quality of each algorithm based on the RMSE they produce. As mentioned before, the thresholds are really tight because the estimated spectrum must be as close to the original as possible for it to be useful.

### 3.5.3 Algorithms scoring

The same weights are kept for the second experiments as well(70% for the amount of bands needed and 30% for the time needed). Also, the same thresholds as mentioned in tables 3.2, 3.3 hold for the points given for each algorithm.

Lastly, again, if an algorithm fails to reach a quality criterion a penalty is given so the count of the bands needed increases. This count is the same as table 3.4.

These are the scores for the algorithms:

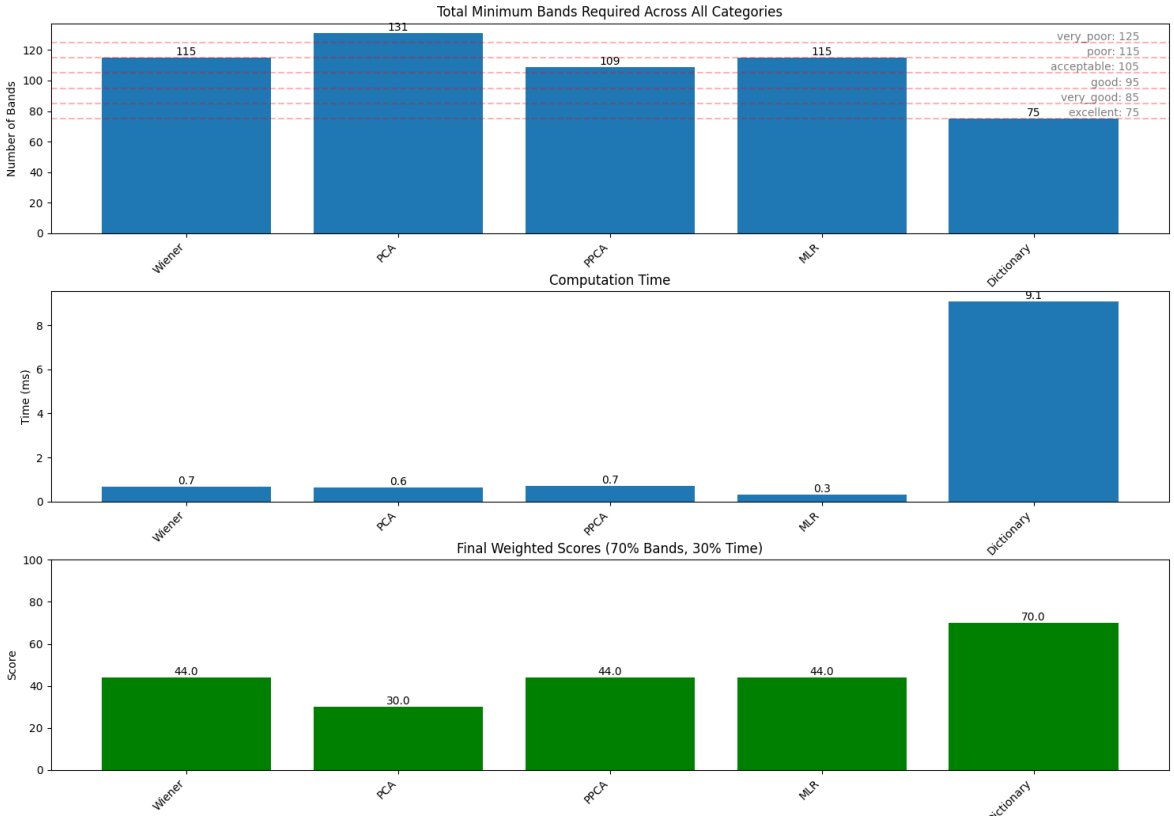


Figure 3.34: Algorithms Scores

Below we present the total results for each algorithm will be presented, in order to give a better view of how good estimation each algorithm makes and how consistent it can be.

| **Quality** | **Wiener** | **PCA** | **PPCA** | **MLR** | **Dictionary** |
|---|---|---|---|---|---|
| Excellent | 51 | not reached | not reached | 51 | 31 |
| Very Good | 16 | not reached | 26 | 17 | 12 |
| Good | 14 | 16 | 14 | 13 | 10 |
| Acceptable | 12 | 14 | 12 | 12 | 9 |
| Poor | 11 | 13 | 11 | 11 | 7 |
| Really Poor | 11 | 13 | 11 | 11 | 7 |

Table 3.7: Score of all algorithms

### 3.5.4 Discussion about Results

There are plenty of things to talk about by observing the results and the scores of the second experiment.

- First of all, we can see that a jump on the minimum bands required across all categories for all the algorithms except Dictionary Learning. This can be explained by the nature of the experiment. The models are trained using the Macbeth Color Checker, when data are smooth and calibrated. The validation is using spectra from real life images which is not ideal, therefore the model cannot estimate them accurately with as few bands as before. For that reason we can see that the scores are low.

- Dictionary Learning seems to estimate better because the atoms, that are produced in training, are simpler and can reconstruct the natural spectra more easily. This happens due to the fact that these atoms are more general than the atoms that the first experiment produces and a mix of those simple atoms can reconstruct the natural spectra.

- Using these datasets for training-validation, we can see that the algorithm that achieves the best score and uses fewer bands is Dictionary

Learning. Nevertheless, the score achieved by Dictionary Learning is not good enough to be confident on its estimation, but among the algorithms it's the best choice.

- Dictionary Learning is the only method that achieves better score in this experiment but still, even though the training files are cached, it takes a lot of time to produce a result because the number of atoms used(100) results in many multiplications so more processing time.
- We can see that still Wiener,PPCA and MLR still produce better results than PCA and are similar to one another.
- 2 out of 5 algorithms (PCA, PPCA) fail to reach excellent estimation. PCA even fail to reach very good quality, which makes this method very unreliable.
- As we can see from the spectra comparisons of the algorithms it is clear that they struggle a lot more than in Experiment 1. The produced spectra are clearly less accurate than before and again the main spikes in RMSE are around 400 to 460 nm and 670 to 730nm.

## 3.6 Conclusions

The Experiments try to tackle the same problem using the same datasets for different reasons.

In the first Experiment, we can see that by using the reflectances of natural objects for the training set and the Macbeth Color Checker as validation set, the scores, and hence the estimations, can be really good, thus trustworthy. On the other hand, in the second Experiment we can see that by using Macbeth as training set and natural objects as validation the results are not so good.

Let's analyze a little more why the above results are expected. Natural objects cover a much broader and more complex range of spectral shapes

than Macbeth patches. Macbeth Color Checker patches are a set of 140 standardized color samples, designed to cover a wide range of colors.However, they are still a limited, artificial set. When we train our model on Macbeth patches, it learns to reconstruct or estimate spectra that are similar to those patches.

If the spectra from natural objects have features (shapes, peaks, valleys, or overall distributions) that are not well represented in the Macbeth set, the model will struggle to generalize. This leads to higher errors (lower scores) when evaluated on natural spectra. Also, Macbeth patches are designed for color calibration, not for representing the full diversity of natural reflectance spectra. The statistical properties (mean, variance, correlations between bands) of the Macbeth set are different from those of natural spectra. Macbeth set can be viewed as a subset of natural spectra, together with the fact that many spectral estimation methods (Wiener, PCA, PPCA, etc.) rely on these statistics results in the conclusion that the statistics that Macbeth patches provide to the model are insufficient for the model to be able to reproduce natural spectra. However, Dictionary Learning is not based on those statistics and is more based on the nature and the complexity of the spectra. That's why being trained in simpler data, like Macbeth patches, makes the atoms of the Dictionary more agile and easier to fit in the more complex spectra of natural objects.

On the other hand, natural spectra are more diverse. This means that when our models are trained with that set they learn to handle a wider variety of spectral features (sharp edges, broad bands, unique pigment signatures, etc.). Additionally, the Macbeth Color Checker patches are a small, controlled subset of possible spectra. They are designed to be representative for color calibration, but they are much simpler and less variable than natural spectra so when the model is trained on the complexity of natural objects it can easily handle the simpler, more regular Macbeth patches. Training on a broad, diverse dataset (natural spectra) allows the model to generalize

well to any subset, including the Macbeth patches. Ultimately, the statistical space covered by the natural objects set include Macbeth patches, but not vice versa. Practically this means that the model trained on natural spectra has "seen" examples similar to Macbeth patches, while the reverse does not hold true. In this case however, the atoms of the Dictionary become more specialized and overfitted and can't match the ideal-smoothed Macbeth patches.

The above makes sense in the following way as well : The natural spectra is a generalization and combination of the Macbeth patches. So learning the general helps the model to acknowledge the specific where the opposite obviously can not hold true in this problem.

# Chapter 4

# Conclusions and Future Work

In this thesis we studied and compared the performance of some methods for spectral estimation and how they behave with less and less sample bands.

In Chapter 1 we made an introduction to the topic of HyperSpectral and MultiSpectral imaging. We analyzed the techniques of HyperSpectral Data Acquisition and the way Spectral Cubes are created. Also, we show that Color Imaging systems are not able to distinguish material with the same color appearance but different chemical composition due to the effect of metamerism. We pointed out that the difference of MultiSpectral imaging to HyperSpectral is the number of bands each system uses, with the HyperSpectral being able to use more bands therefore it can produce better results. Then, we emphasized the importance of spectral Estimation methods due to the fact that spectral imagers are not able to obtain a big number of wavelengths without losing spatial resolution.

In Chapter 2 we analyzed the problem of spectral Acquisition and Estimation. We modeled it and explained the mathematical terms of the model. Then, we introduced some well known Spectral Estimation methods and made the theoretical analysis of each model. We also made clear why we train our models with these methods and what do the models learn with training.

In Chapter 3, Two different experiments were made using Macbeth Color Checker and a Spectral dataset of natural objects reflectances. Using MUSES9-

HS Camera, images from 400nm (UV) to 1000(NI) were taken of Macbeth Color Checker and were used for the experiments. In the first experiment we used the dataset of objects as training set and Macbeth Color Checker as validation set and in the second vise versa. We performed estimation with each method using from 121 to 7 sample bands. In the first experiment, we saw that Wiener, PPCA and MLR methods performed well, especially when the training file was cached. The results of those methods were pretty good and those three methods produced trustworthy results. In the second experiment, we saw a significant drop in performance and this time the most reliable method came out to be Dictionary Learning, even though this method also failed to score high.

From the experiments we made several observations regarding the datasets and the behavior of the algorithms. We saw that the models that are based on the statistics, perform better when trained with spectra from natural objects due to the fact that these spectra contain more diverse information about the statistical properties of spectra as well as the spectral features. Macbeth Color Checker patches are a small, controlled subset of possible spectra. They are designed to be representative for color calibration, but they are much simpler and less variable than natural spectra so when the model is trained on the complexity of natural objects it can easily handle the simpler, more regular Macbeth patches. On the other hand, Dictionary Learning which does not rely on statistics seems to work better when trained with simpler data like Macbeth patches.

The validation and the scoring of this thesis was also based on the time that these methods need to perform. We tried to evaluate the methods in order to be able to be used in a real time system and also produce accurate results. Our goal is a snapshot imager that doesn't have a trade off between time and quality of the result in contrast to the color imagers that are used today. These imagers need to sacrifice spectral resolution by using really broad bands in order to produce results in real time.

More methods could be tested based on this system of evaluation in order for the best method to be decided. Methods like Local Wiener, Kernel Regression or some types of neural networks(CNN's and ANN's) could be used in this type of problem and could be interesting fields for future work.

# Bibliography


[1] NIREOS. [Online]. Available: https://nireos.com/application/what-is-hyperspectral-imaging/.

[2] National Oceanic and Atmospheric Administration. [Online]. Available: https://www.noaa.gov/jetstream/satellites/electromagnetic-waves.

[3] LeaderTech. [Online]. Available: https://leadertechinc.com/basics-electromagnetic-spectrum/.

[4] Lorenzo Cotrozzi. Spectroscopic detection of forest diseases: a review (1970-2020). *Journal of Forestry Research*, 2021. [Online]. Available: https://www.researchgate.net/publication/353908965_Spectroscopic_detection_of_forest_diseases_a_review_1970-2020.

[5] Schmidt Academy for Software Engineering. [Online]. Available: https://commons.wikimedia.org/wiki/File:Multispectral_imaging_approaches.svg.

[6] Schmidt Academy for Software Engineering. [Online]. Available: https://sase.caltech.edu/projects/wiser.html/.

[7] Alamin Mansouri, Tadeusz Sliwa, Jon Yngve Hardeberg, and Yvon Voisin. An adaptive-pca algorithm for reflectance estimation from color images. In *2008 19th International Conference on Pattern Recognition*, pages 1–4, 2008.

[8] X-rite. [Online]. Available: https://www.xrite.com/categories/calibration-profiling/colorchecker-digital-sg.

[9] Spectricon. [Online]. Available: https://spectricon.com/products-and-markets/muses-9-hs.

[10] P. Stigell, K. Miyata, and M. Hauta-Kasari. " wiener estimation method in estimating of spectral reflectance from rgb images". *Pattern Recognition and Image Analysis*, 17:233–242, 2007. [Online]. Available: https://doi.org/10.1134/S1054661807020101.

[11] Kensuke Sekihara and Bernard Scholz. Generalized wiener estimation of three-dimensional current distribution from biomagnetic measurements. *IEEE Transactions on Biomedical Engineering*, 43(3):281–291, Mar 1996. [Online]. Available: https://doi.org/10.1109/10.486285.

[12] Xiaoyu Cui Shuo Chen, Gang Wang and Quan Liu. Stepwise method based on wiener estimation for spectral reconstruction in spectroscopic raman imaging. 25(2):1005–1018, 2017. [Online]. Available: https://doi.org/10.1364/OE.25.001005.

[13] Kyuichi Niizeki Yoshihisa Aizu Izumi Nishidate, Takaaki Maeda. Estimation of melanin and hemoglobin using spectral reflectance images reconstructed from a digital rgb image by the wiener estimation method. *Sensors 2013*, 13(6):7902–7915, 2013. [Online]. Available: https://doi.org/10.3390/s130607902.

[14] Masahiro Yamaguchi Yuri Murakami and Nagaaki Ohyama. Piecewise wiener estimation for reconstruction of spectral reflectance image by multipoint spectral measurements. *Appl. Opt*, 48(11):2188–2202, 2009. [Online]. Available: https://doi.org/10.1364/AO.48.002188.

[15] Roy S. Berns Yonghui Zhao. Image-based spectral reflectance reconstruction using the matrix r method. *Wiley Periodicals, Inc. Col Res*

*Appl*, 32:343–β351, 2007. [Online]. Available: https://doi.org/10.1002/col.20341.

[16] Stiles WS Wyszecki G. High-level trichromatic color matching and the pigment-bleaching hypothesis. *Vision Res*, 20:23–37, 1980. DOI: 10.1016/0042-6989(80)90138-8.

[17] Leyuan Fang, Shutao Li, Ryan P. McNabb, Qing Nie, Anthony N. Kuo, Cynthia A. Toth, Joseph A. Izatt, and Sina Farsiu. Fast acquisition and reconstruction of optical coherence tomography images via sparse representation. *IEEE Transactions on Medical Imaging*, 32(11):2034–2049, 2013.

[18] Snir Gazit, Alexander Szameit, Yonina C. Eldar, and Mordechai Segev. Super-resolution and reconstruction of sparse sub-wavelength images. *Opt. Express*, 17(26):23920–23946, Dec 2009.

[19] Yi-Tun Lin and Graham D. Finlayson. A rehabilitation of pixel-based spectral reconstruction from rgb images. *Sensors*, 23(8), 2023.

[20] Yi Chang, Luxin Yan, Houzhang Fang, Sheng Zhong, and Wenshan Liao. Hsi-denet: Hyperspectral image restoration via convolutional neural network. *IEEE Transactions on Geoscience and Remote Sensing*, 57(2):667–682, 2019.

[21] Shaohui Mei, Xin Yuan, Jingyu Ji, Yifan Zhang, Shuai Wan, and Qian Du. Hyperspectral image spatial super-resolution via 3d full convolutional neural network. *Remote Sensing*, 9(11), 2017.

[22] Liangliang Song, Zhixi Feng, Shuyuan Yang, Xinyu Zhang, and Licheng Jiao. Self-supervised assisted semi-supervised residual network for hyperspectral image classification. *Remote Sensing*, 14(13), 2022.

[23] Jong-Il Park, Moon-Hyun Lee, Michael D. Grossberg, and Shree K. Nayar. Multispectral imaging using multiplexed illumination. In *2007 IEEE 11th International Conference on Computer Vision*, pages 1–8, 2007.

[24] Xiaolin Han, Jing Yu, Jiqiang Luo, and Weidong Sun. Reconstruction from multispectral to hyperspectral image using spectral library-based dictionary learning. *IEEE Transactions on Geoscience and Remote Sensing*, 57(3):1325–1335, 2019.

[25] Oğuzhan Fatih Kar and Figen S. Oktem. Compressive spectral imaging with diffractive lenses. *Opt. Lett.*, 44(18):4582–4585, Sep 2019.

[26] Hui-Liang Shen, Hui-Jiang Wan, and Zhe-Chao Zhang. Estimating reflectance from multispectral camera responses based on partial least-squares regression. *Journal of Electronic Imaging*, 19(2):020501, 2010.

[27] Mirko Agarla, Simone Bianco, Marco Buzzelli, Luigi Celona, and Raimondo Schettini. Fast-n-squeeze: Towards real-time spectral reconstruction from rgb images. In *Proceedings of the IEEE/CVF Conference on Computer Vision and Pattern Recognition (CVPR) Workshops*, pages 1132–1139, June 2022.

[28] Mirko Agarla, Simone Bianco, Luigi Celona, Raimondo Schettini, and Mikhail Tchobanou. An analysis of spectral similarity measures. *Color and Imaging Conference*, 29(1):300–300, 2021.

[29] Xiaorui Song and Lingda Wu. Hyperspectral image inpainting based on robust spectral dictionary learning. *Applied Sciences*, 9(15), 2019.

[30] Mingrui Yang, Frank de Hoog, Yuqi Fan, and Wen Hu. Compressive hyperspectral imaging via adaptive sampling and dictionary learning, 2015.

[31] Jingjing Liu, Wanquan Liu, Qilin Li, Shiwei Ma, and Guanghua Chen. Evaluation of k-svd with different embedded sparse representation algo-

rithms. In *2016 12th International Conference on Natural Computation, Fuzzy Systems and Knowledge Discovery (ICNC-FSKD)*, pages 426–432, 2016.

[32] Michael E. Tipping and Christopher M. Bishop. Probabilistic principal component analysis. *Journal of the Royal Statistical Society Series B: Statistical Methodology*, 61(3):611–622, 01 2002.

[33] MARCELO AGUSTΓN GUTIΓRREZ, BΓ‘rbara Silva, Jose Maria Fanchini, Takuma Morimoto, Pablo Barrionuevo, and MarΓa Leonor Sandoval Salinas. Spectral dataset of natural objectsβ reflectance from the Southern cone ofB SouthB America. 4 2024.